A buffering mechanism against genetic perturbations in gene expression

2017, March

Koji Ishikawa

Graduate School of Natural Science and Technology

Doctor's Course

OKAYAMA UNIVERSITY

Table of Contents

Abbreviations

CHX: cycloheximide

GFP: green fluorescent protein

gTOW: genetic tug-of-war

mRNA: messenger RNA

OD_{600}: optical density at 600 nm

PAP: peroxidase anti-peroxidase soluble complex

RNA-seq: RNA sequencing

rRNA: ribosomal RNA

SC–Leu–Ura: synthetic complete medium lacking leucine and uracil

SC–Ura: synthetic complete medium lacking uracil

TAP: tandem affinity purification

TEV: tobacco etch virus

Abstract

Understanding buffering mechanisms for various perturbations is essential for understanding robustness in cellular systems. Protein-level dosage compensation, which arises when changes in gene copy number do not translate linearly into protein level, is one mechanism for buffering against genetic perturbations. Here, I present an approach to identify genes with dosage compensation by increasing the copy number of individual genes using the genetic tug-of-war technique. A screen of *Saccharomyces cerevisiae* chromosome I suggests that dosage-compensated genes constitute approximately 10% of the genome and consist predominantly of subunits of multi-protein complexes. Importantly, because subunit levels are regulated in a stoichiometry-dependent manner, dosage compensation plays a crucial role in maintaining subunit stoichiometries. Indeed, changes in the levels of a complex were observed when its subunit stoichiometries were perturbed. I further analyzed compensation mechanisms using a proteasome-defective mutant and autophagy-defective mutants as well as ribosome profiling, which provided strong evidence for compensation by ubiquitin-dependent degradation but not by autophagy and reduced translational efficiency. Thus, this study provides a systematic understanding of dosage compensation and highlights that this post-translational regulation is a critical aspect of robustness in cellular systems.

Chapter 1

General introduction

1.1 Robustness of cellular systems

Robustness in biological systems is a general trait of living cells and a fundamental feature involving the maintenance of stability during perturbation [1–4]. It is a universal challenge to cope with perturbations leading to fluctuations in biological processes because cells are exposed to changes in internal and external environments [5,6]. Under stress conditions, cells change gene expression levels in order to activate appropriate stress response mechanisms. By such mechanisms, stability in perturbed systems and growth is recovered, and finally cells adapt to stress conditions. While adaptation is a consequence of robustness, fragility indicates a lack of robustness. If cells experience one perturbation and develop responses to it, adaptation to the perturbation is possible. On the other hand, if cells are not able to buffer one perturbation and to develop responses to it, adaptation to the perturbation is impossible. At the same time, cells may lose and obtain a potential opportunity to adapt to the other perturbation in the former and latter cases, respectively. Therefore, this relationship is expressed as the trade-off between robustness and fragility.

Changes in gene expression levels are achieved through various mechanisms in the whole process of gene expression (Figure 1.1). This is a source of stress response and adaptation as described above, so that one aspect of the cellular robustness to various perturbations can be understood as a consequence of fluctuations in gene expression and buffering of fluctuations [5–8], as illustrated in Figure 1.2. For example, alterations in gene copy number are known as a source of such fluctuations, which is one of the hallmarks of cancer cells and the cause of Down's syndrome [9]. Therefore, under-

standing buffering mechanisms is essential to understanding the optimization of gene expression and adaptation to changes in environmental conditions. Investigations of mechanisms conferring robustness to cellular systems have proceeded by regarding a cell as a single system. In this context, each of the cellular elements (e.g., genome, transcriptome, proteome, metabolome) is recognized as a parameter in biological processes. It is important to study changes in each of the parameters, which is representative of gene expression, in response to various perturbations because of the fact that in the face of perturbations gene expression dynamically changes to maintain cellular homeostasis. This recognition is a philosophical foundation of Systems Biology.

1.2 Consequences of genetic perturbations

As a consequence of genetic perturbations in gene expression, protein synthesis and degradation deviate from the steady state. This cellular state has recently been proposed as proteome imbalance [10]. Protein overexpression leads to proteome imbalance and causes cellular defects depending on properties and functions of proteins [11]. The causal mechanisms have been classified into four types: resource overload, stoichiometric imbalance, promiscuous interactions, and pathway modulation [12]. Briefly, for example, resource overload, stoichiometric imbalance, promiscuous interactions, and pathway modulation may cause the protein burden effect, abnormal complex formation, sequestration of essential proteins, and abnormal regulation of transcription and signaling pathway, respectively. These mechanisms are regarded as the primary ones responsible for cellular defects due to protein overexpression. In this study, I focused on the stoichiometric imbalance as described below.

Proteome imbalance has been proposed to cause proteotoxic stress through those mechanisms. Proteotoxic stress is induced by an increased burden on the systems for the protein quality control, including molecular chaperone networks and degradation

pathways, due to excess proteins [13,14]. As characteristic features of proteotoxic stress, cells with proteotoxicity are sensitive to inhibition of protein synthesis and folding and show metabolic alterations [15]. Proteotoxic stress is closely related with the formation of protein aggregates; indeed, proteins are prone to form aggregates in aneuploid yeast strains containing an extra chromosome [16]. Furthermore, a deletion of the deubiquitinase gene *UBP6* in the aneuploid strains decreased the number of cells with aggregates. While some aneuploid yeast strains were shown to grow very slowly, a deletion of *UBP6* suppressed the proliferation defect of these strains [15]. These observations suggest that activation of ubiquitin-dependent degradation of excess proteins rescues cell growth under genetic perturbations causing proteotoxic stress.

1.3 Measurement of cell robustness against gene overexpression

The molecular mechanisms conferring robustness to some biological processes have been studied (e.g., cell cycle, circadian clock). However, we lack a method allowing an assessment of robustness of cell fitness in global, systematic, and quantitative manners. This demand has been addressed by some studies, and the molecular and physiological phenotypes have been connected to achieve a global measurement of cell robustness [17–20]. For example, systematic investigations of the robustness in cellular systems have been performed by focusing on the effects of manipulating gene copy number on cell growth [18,19]. These studies based on gene copy number increase mainly used two different approaches: introducing a plasmid carrying an individual target gene [18] and generating aneuploidy of specific chromosomes [19]. The former study measured cell robustness to gene overexpression using a genetic technique termed genetic tug-of-war (gTOW), by which fragility to protein overproduction is indirectly and quantitatively assessed as an upper limit of gene copy number in *Saccharomyces cerevisiae* [18,21,22]. Moriya et al [21] developed the gTOW technique in order to measure cell robustness

against gene overexpression and shed light on how we can explore its quantitative aspects. The gTOW technique is a method of relative overexpression in contrast to the fact that a promoter-swapping technique (e.g., the use of *GAL1* and *TDH3* promoters) is one of the methods of absolute overexpression. A promoter-swapping technique increases messenger RNA (mRNA) level and the increase strongly depends on the promoter activity. As it is impossible to compare mRNA levels expressed from the native promoter and the non-native one in the same cells, we cannot determine the fold increase in gene expression level. On the other hand, the gTOW technique, a method of the relative overexpression, allows us to measure how many folds the gene expression level increase compared with the native level. The relative overexpression method is useful to quantitatively assess robustness of cell systems against gene overexpression. The genome-wide gTOW analysis has revealed fragile points as a set of 115 dosage-sensitive genes that cause impaired growth when the gene copy number is slightly increased [18]. In other words, only 2% of the yeast genome (115 out of 5806 genes) is sensitive to gene dosage such that a copy number increase leads to breakdown of biological systems. Conversely, this result indicates that genetic perturbations to biological processes are generally buffered. However, the buffering mechanisms behind the robustness against gene overexpression remain to be investigated. On the other hand, the latter studies using aneuploid yeast and mammalian cells have also revealed fragility of cellular systems against gene copy number increase in a genome-wide manner [19]. Further analysis has shown that the fragility of aneuploid cells is caused by many genes on single additional chromosomes but not by the dosage-sensitive genes duplicated by ploidy changes [23]. Moreover, previous studies have demonstrated the effects of aneuploidy on cell fragility (e.g., growth impairment caused by proteotoxic stress, hypersensitivity to inhibitors of protein synthesis, folding, and degradation) [15,24,25], while an increase in individual gene copy number generally does not cause a defect in cell

growth [18]. These findings indicate differences of impact on cell robustness between many copies of a single gene and an additional chromosome. I thus expect that exploring the effects of an increase in individual gene copy number will identify novel mechanisms for maintaining cell homeostasis.

1.4 Protein-level dosage compensation is one mechanism for buffering against genetic perturbations

Global analyses of cell robustness against gene overexpression have revealed that cells tend to be fragile upon an increase in the copy number of genes encoding subunits of multi-protein complexes [17,18]. This is analogous to a previous study that predicted deleterious effects caused by an imbalance in subunit stoichiometries in complexes [26]. Interestingly, studies on aneuploidy have demonstrated that the copy number of a subset of genes, enriched in subunit-encoding genes, correlates with mRNA levels but not directly with protein levels. This phenomenon is known as protein-level dosage compensation, reported in yeast and mammalian cells [9,24,27], which is illustrated in Figure 1.3. The first example of genes with protein-level dosage compensation may be tubulin genes in *S. cerevisiae* [28]. This study manipulated the copy number of alpha-tubulin genes *TUB1* and *TUB3* and beta-tubulin gene *TUB2* and measured changes in the protein level for each gene in some different copy number conditions. The level of Tub1 protein increased to only 119% and 150% of wild-type level in the extra *TUB1* (carrying an additional copy of *TUB1*) and *TUB1+2* (carrying an additional copy of *TUB1* and *TUB2*) strains, respectively. The level of Tub2 protein also increased to only 115% of wild-type level in the extra *TUB1+2* strain, while it was 92% in the extra *TUB1* strain. Additionally, the level of Tub3 protein decreased to 74% and 88% of wild-type level in the extra *TUB1* and *TUB1+2* strains, respectively.

Recent study using ribosome profiling technique [29] has shown that transla-

tional efficiency of genes encoding subunits in a complex corresponds to a stoichiometry of the subunits [30]. This phenomenon is called a proportional synthesis strategy and guarantees stoichiometry of almost all the 18 well-characterized complexes tested in this study, with a small number of exceptions synthesized in excess (Srp54 and Sec65 in the signal recognition particle). Protein-level dosage compensation is expected to reduce excess subunits and directly contribute to maintaining the subunit stoichiometry. Because stoichiometric imbalance is a consequence of proteome imbalance, dosage compensation is believed to play an important role for circumventing the imbalance and confer robustness to cell systems.

1.5 Aim and scope of this study

In this study, I developed a screening system based on the gTOW technique for the following aims: (i) to systematically identify genes with dosage compensation upon an increase in gene copy number, and (ii) to estimate how much of the genome is subjected to dosage compensation. Findings from this study suggest that the proportion of the dosage-compensated genes in the genome is approximately 10% and these genes may encode subunits of protein complexes. I also investigated the compensation mechanism by focusing not only on protein degradation but also on translational efficiency by using a ribosome profiling technique [29]. This study suggests that the robustness of gene expression reflects transient degradation, dynamic changes in protein lifetime, produced in response to environmental changes. Furthermore, this study provides insight into the mechanisms for coping with the fluctuations in biological processes caused by gene copy number alterations. I believe that the effect of alterations in gene copy number is one of the fundamental issues in genetics. Similarly, studies on the mechanisms for buffering against genetic perturbations may lead to a deeper understanding of cell homeostasis in the context of robustness. In particular, this study may be useful for study-

ing the robust formation of protein complexes. I also believe that the approach based on the gTOW technique provides a quantitative measurement of robustness in cellular systems.

1.6 Figures

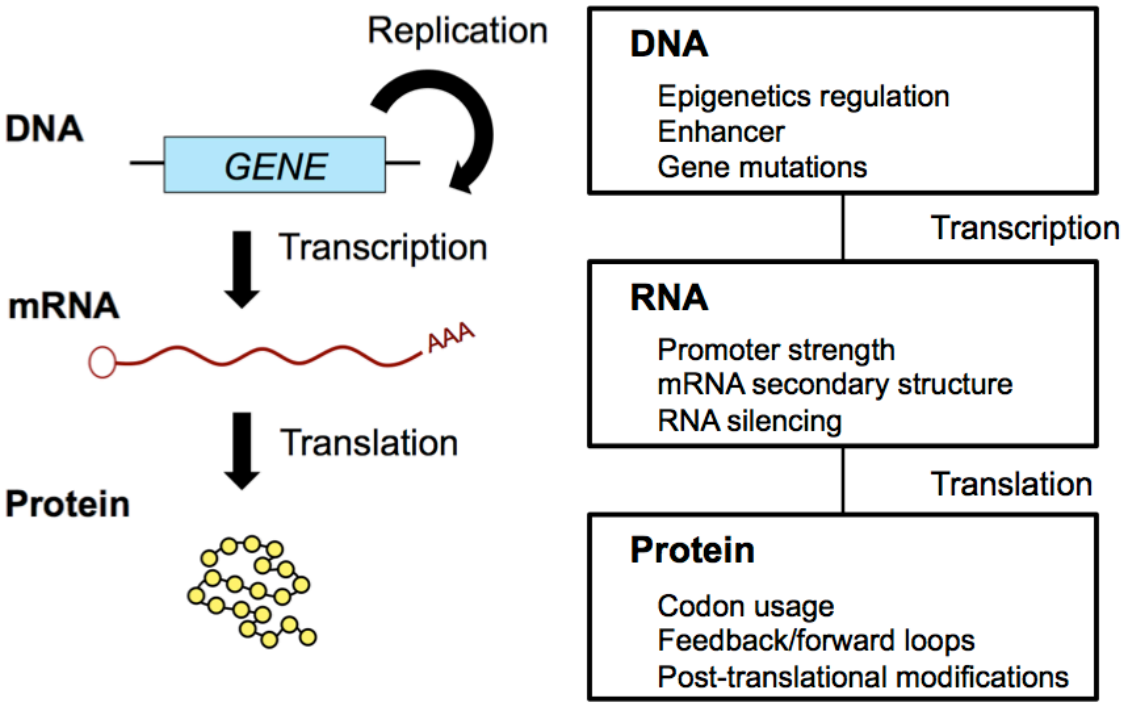

Figure 1.1. Gene expression processes and various mechanisms for regulating gene expression levels.

Gene expression is ultimately a process for producing functional proteins (left panel). Gene expression levels are regulated by various mechanisms at each step of gene expression, and some of them are listed in the right panel.

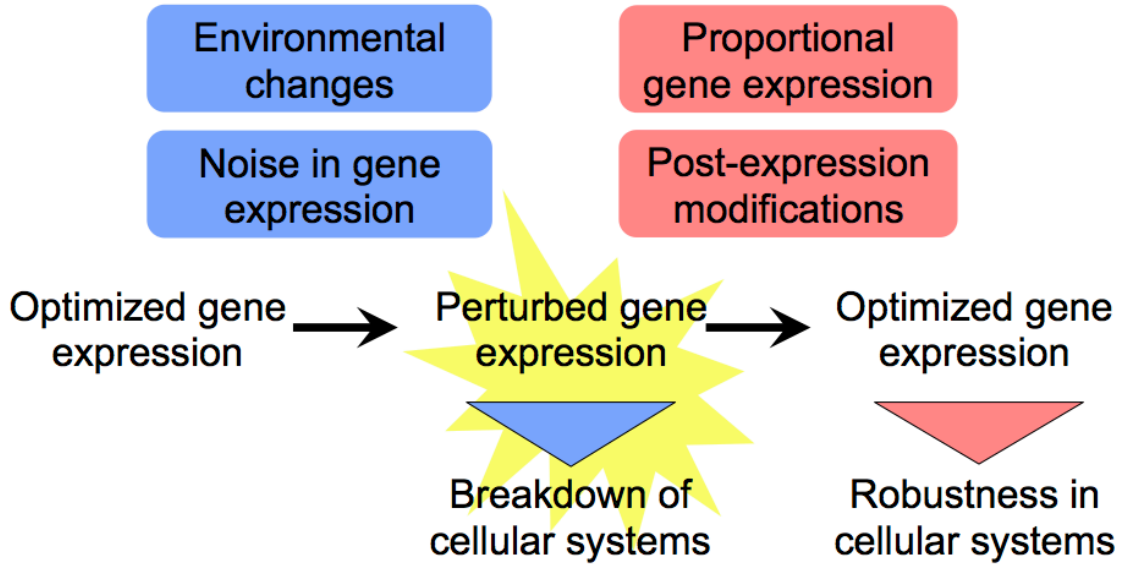

Figure 1.2. Schematic understanding of the relationship between gene expression and cell robustness.

Because cells are exposed to environmental changes and biological processes are not deterministic, gene expression fluctuates not only in stress conditions but also in physiological conditions. If such perturbed gene expression is not buffered, it may result in breakdown of cellular systems. On the other hand, if the perturbed gene expression is buffered, and optimized gene expression is maintained, it can achieve robustness in cellular systems. Therefore, fluctuations and optimization of gene expression may be critical for cellular robustness.

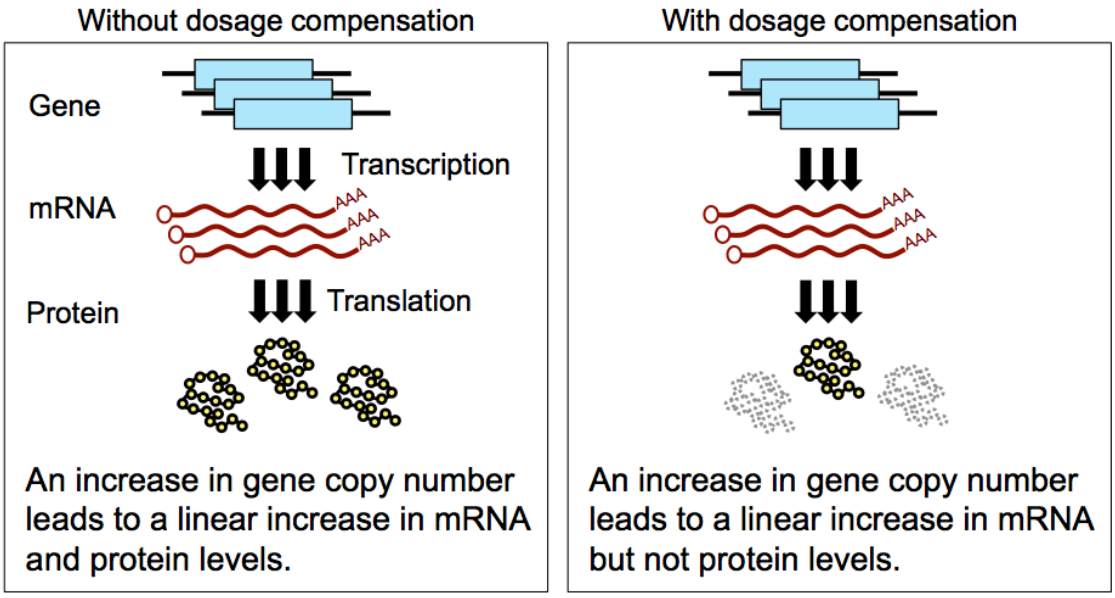

Figure 1.3. Protein-level dosage compensation.

Majority of the genome shows a proportional increase in mRNA and protein levels when their gene copy number increases, as shown in the left panel. On the other hand, a small subset of the genome is subjected to dosage compensation at the protein level, as shown in the right panel.

Chapter 2

Screening system to identify the dosage-compensated genes

2.1 Introduction

The decoding of genetic information is achieved through irreversible processes from DNA to RNA to protein as stated in the central dogma of molecular biology [31]. The gene expression level at each step is generally in a linear relationship with gene copy number, namely an increase in gene copy number leads to a proportional increase in mRNA and corresponding protein levels. However, in the face of perturbations, this linear relationship should become nonlinear for maintaining cellular homeostasis. This prediction highlights the importance of studying the quantitative aspects of the central dogma in the context of robustness. For example, previous studies have demonstrated that a small subset of genome shows protein-level dosage compensation upon genetic perturbations. A remarkable study using aneuploid yeast cells has revealed that approximately 20% of the yeast genome is subjected to dosage compensation [19]. This study used haploid *S. cerevisiae* that contains 16 chromosomes and analyzed 13 out of 16 disomic strains that carry each of the additional chromosomes. Although this analysis provides a systematic understanding of dosage compensation, some hallmarks of aneuploidy have raised the need of identification of the dosage-compensated genes in normal physiological condition. In aneuploid cells, protein synthesis and degradation networks are perturbed by excess amount of proteins, and as a consequence of proteome imbalance, the cells are exposed to proteotoxic stress that causes cell fragility leading to growth impairment. Indeed, many of disomic strains are sensitive to inhibitors of protein synthesis cycloheximide (CHX), hygromycin, and rapamycin and to proteasome inhibitor MG-132 compared with wild-type cells [25]. Moreover, they are sensitive to

geldanamycin, an inhibitor of a molecular chaperone Hsp90, suggesting the effects of aneuploidy on protein folding and the broad impact of proteome imbalance caused by aneuploidy. Interestingly, a recent study has shown that the fragility of aneuploid cells is caused by many genes on single additional chromosomes but not by duplicated dosage-sensitive genes that were identified by the gTOW analysis [23]. As described above, the genome-wide gTOW analysis has revealed that yeast cells grow robustly upon an individual increase in the copy number of approximately 98% of the yeast genome. Therefore, I developed an experimental setup based on the gTOW technique for screening of genes with protein-level dosage compensation in order to ask how much of the yeast genome is compensated.

2.2 Materials and Methods

2.2.1 Strains

The yeast strain BY4741 (*MATa his3Δ1 leu2Δ0 met15Δ0 ura3Δ0*) [32] was used for the screening. Nucleotide sequence encoding the tandem affinity purification (TAP) (the detail components of the TAP tag is shown in Figure 2.1) or green fluorescence protein (GFP) tags were integrated into the 3´-region of each gene [33].

2.2.2 Plasmids

A target gene with native regulatory regions, including promoter and 5´ and 3´ untranslated regions, is cloned into a multicopy plasmid, pTOWug2-836 or pTOW40836 [18]. As shown in Figure 2.2, these plasmids contain *leu2-d* and *URA3* genes as selective markers, so that yeast cells carrying this plasmid can be selected on synthetic complete medium lacking uracil (SC–Ura) or one lacking leucine and uracil (SC–Leu–Ura) media.

2.2.3 Transformation of yeast cells

Yeast strains were transformed by the lithium acetate method as described previously [34] with modifications. Yeast cells grown in YPD medium were harvested at log-phase and washed with sterile water. The cells were treated with 1 M lithium acetate at room temperature for 4 min, and then, sonicated salmon sperm DNA, plasmid, and 50% polyethylene glycol were added to the cells. After mixing them, the mixture was incubated at room temperature for 30 min and 42 °C for 20 min, and then the cells were plated on SC–Ura plate and grown at 30 °C for a couple of days. The transformants were grown with shaking at 30 °C in SC–Ura or SC–Leu–Ura media.

2.2.4 Western blot analysis

Yeast cells were grown in 2 mL of the appropriate medium and subcultured in 3 mL of fresh medium. The optical density at 600 nm (OD_{600}) was measured and 2 OD_{600} units were harvested at log-phase. The cells were treated with 1 mL of 0.2 N NaOH for 5 min at room temperature and then were suspended in 2× NuPAGE LDS Sample Buffer (Invitrogen) and heated at 70 °C for 10 min. The supernatant corresponding to 0.5 OD_{600} units was labeled with EzLabel FluoroNeo (ATTO) and subjected to SDS-PAGE, followed by Western blotting with PAP (Sigma-Aldrich) (1:2000) or an anti-GFP antibody (Roche) (1:1000) and peroxidase-conjugated secondary antibody (Nichirei Biosciences) (1:1000). NuPAGE 4%–12% Bis-Tris Gel (Invitrogen) and iBlot Transfer Stack PVDF membrane (Invitrogen) were used for SDS-PAGE and Western blotting, respectively. Chemiluminescence was induced by SuperSignal West Femto Maximum Sensitivity Substrate (Thermo Scientific) and detected using LAS-4000 image analyzer (Fujifilm) and ImageQuant LAS 4000 (GE Healthcare). The band intensity was quantified using ImageQuant TL (GE Healthcare), and the fold change of protein levels was calculated with a previously described method [35].

2.2.5 Analysis of mRNA expression levels

Yeast cells grown in the appropriate medium were harvested at log-phase and subsequently total RNA was extracted using the hot phenol method [36]. Contaminating genomic DNA was removed and reverse transcription was carried out with PrimeScript RT reagent Kit with gDNA Eraser (TaKaRa) according to the manufacturer's instructions. The generated cDNA was amplified by real-time quantitative PCR with Lightcycler 480 using SYBR Green I Master. Quantification of *TAP* tag and *ACT1* mRNA expression was performed with the following primers to amplify *TAP*-tag and *ACT1* gene on the chromosome: *TAP*-tag-forward (5´-AATTTCATAGCCGTCTCAGCA-3´); *TAP*-tag-reverse (5´-CTCGCTAGCAGTAGTTGGAATATCA-3´); *ACT1*-forward

(5´-TGCAAACCGCTGCTCAA-3´); and *ACT1*-reverse (5´-TCCTTACGGACATCGACATCA-3´). The fold change of mRNA levels was calculated as previously described [35].

2.2.6 Measurement of gene copy number

The copy number of each gene was measured using the gTOW technique, as described previously [18]. Briefly, single colonies of yeast cells carrying pTOW plasmids were cultivated in a 96-well plate containing 200 μL of SC–Ura medium for 4 days at 30 °C, and then, 5 μL of the culture was inoculated into 200 μL of fresh SC–Ura medium. After culturing for 50 h at 30 °C, the cells were harvested by filtration followed by DNA extraction with zymolyase treatment. The extracts were subjected to real-time quantitative PCR with Lightcycler 480 (Roche) using SYBR Green I Master (Roche) to quantify the expression of *LEU3* from the chromosome and *leu2d* gene from pTOW plasmids. The resulting copy number of the pTOW plasmid carrying each target gene was calculated according to the method described previously [21].

2.3 Results

2.3.1 Identification of the dosage-compensated genes

To identify genes with dosage compensation, I developed a screening method as shown in Figure 2.3A. The key idea of this method is to determine the protein level expressed from a single copy of a target gene when its copy number is increased. I monitored the level of each target protein labeled with the TAP tag expressed from the genomic locus when the copy number of the same target gene without the TAP tag is increased by a multicopy plasmid (Figure 2.3A, middle and right panels). If the expression level of the TAP-tagged protein is reduced in this situation, I consider that the target gene is subjected to dosage compensation (Figure 2.3A, right panel), since the compensation mechanism should not distinguish the TAP-tagged endogenous protein from the non-tagged exogenous protein. Here, I call the condition where the target protein is expressed from the single genomic copy "Single" (Figure 2.3A, left panel) and the condition where the target protein is expressed from the genomic copy and the multicopy plasmid "Multi" (Figure 2.3A, middle and right panels). I used a series of strains in which the TAP tag is integrated into the 3´-region of each gene [33], and a plasmid collection in which each target gene with native regulatory regions, including promoter and 5´ and 3´ untranslated regions, is cloned into a multicopy plasmid, pTOWug2-836 [18].

I examined 54 genes on chromosome I whose TAP-tagged strains were available as representatives of the yeast genome (Table 2.1, Figure 2.4). By this screen, I identified five genes (*RBG1*, *MTW1*, *POP5*, *SAW1*, and *ERP2*) whose protein expression was reduced when their copy numbers were increased (Figure 2.3B). I did not detect off-target effects of an increase in gene copy number by the gTOW technique: the total cellular protein level measured in the total cell lysate did not differ in the Single and Multi conditions. An example of this observation is shown in Figure 2.5A and 2.5C. Quantification of fold change of the protein levels was carried out as shown in Figure

2.5. The protein levels of the dosage-compensated genes were 0.2–0.6-fold (Figure 2.3C), when their copy numbers were 15–27 copies (Figure 2.6). I tested the linearity and accuracy of the Western blot analysis by performing the same analysis using two-fold serially diluted cell lysate (dilution range 1.2 to 0.075 OD_{600} units of cells). The signal intensities of a 50-kDa protein, corresponding to enolase, detected by SDS-PAGE were in a linear relationship with the amount of cell lysate (Figure 2.5A and 2.5C), as well as those of Rbg1-TAP detected by Western blot (Figure 2.5B and 2.5D). I also calculated the fold change as shown in Figure 2.5E and observed dosage compensation in all dilution series (Figure 2.5F). The average of the fold changes in the dilution series and the original data shown in Figure 2.3C was very similar (0.46 and 0.52, respectively). Therefore, I conclude that the quantification had been performed in a linear and accurate manner. Dosage compensations were performed by post-transcriptional regulation because mRNA levels from the endogenous locus did not change even when the copy numbers were increased (Figure 2.3D). Thus, I identified five genes with dosage compensation via post-transcriptional mechanisms.

2.3.2 Observation of dosage compensation in the analysis of endogenous and exogenous protein levels

To verify the experimental setup for measuring only the endogenous protein levels, I measured the level of a target protein expressed from both the genome and plasmid. The experimental setup is the same with that used for the analysis of endogenous protein except that the plasmid encodes each of the TAP-tagged target proteins (Figure 2.7). I measured the total TAP-tagged protein levels (Figure 2.7B and 2.7C) and the plasmid copy numbers (Figure 2.7D) and calculated the fold change of the protein levels per gene copy (Figure 2.7E). This analysis showed dosage compensation of all the five genes identified by the chromosome I screen when considering both endogenous and

exogenous protein levels (Figure 2.7F). The fold change values were very similar with those calculated from the endogenous protein levels. Thus, I conclude that the experimental setup shown in Figure 2.3A, whereby I detect the TAP-tagged protein expressed from the genomic locus, can capture dosage compensation.

2.3.3 Observation of dosage compensation using the GFP tag

I further verified the experimental setup using GFP tag in order to assess the dependency of dosage compensation on the TAP tag. I used the yeast strains in which the GFP tag is integrated into the 3´-region of each target gene and measured the expression levels of GFP-tagged target proteins upon an increase in gene copy number. Western blot analysis for the dosage-compensated proteins Rbg1 and Mtw1 and the uncompensated protein Pop8 showed reduced levels of Rbg1 and Mtw1 but not Pop8 in the Multi condition (Figure 2.8). Because the similar degree of the compensation was observed between the analyses using the TAP and GFP tags, dosage compensation is not a TAP-tag-mediated phenomenon.

2.4 Discussion

I developed a screening method based on the gTOW technique in order to systematically identify the dosage-compensated genes and estimate how much of the genome is subjected to the compensation (Figure 2.3A). The screen of chromosome I showed that 5 out of 54 genes are regulated by the compensation (Figure 2.3B), which estimates that dosage compensation confers robustness to 10% of the genome for buffering perturbed gene expression. As described above, in disomic yeast strains, 20% of the genome is subjected to the compensation at the protein level [19]. This suggests that there are different mechanisms by which cells reduce the level of target proteins for dosage compensation. Indeed, Mtw1, the dosage-compensated proteins identified in this study, is not compensated in aneuploid cells [19]. Previous studies have demonstrated that aneuploidy-induced proteotoxic stress causes cell fragility leading to growth impairment. Thus I expect that there are different rules for determining the target of dosage compensation in the aneuploid condition and that the difference is produced in response to aneuploidy-specific physiological conditions associated with proteotoxicity [13]. I also expect that the gTOW technique allows sensitive detection of the dosage-compensated genes by a much higher increase in copy number of a single target gene than duplication of the same gene in disomic cells.

I verified the screening method for identification of the dosage-compensated proteins by the following two experiments: (i) measuring the total protein levels from the genome and plasmid, measuring the copy number of the plasmid, and calculating protein level per gene copy, and (ii) measuring endogenous protein level with the GFP tag for validation of the results obtained using the TAP tag. First, I analyzed the total levels of a target protein expressed from both a genomic locus and multicopy plasmids. I used a multicopy plasmid encoding each of the TAP-tagged version of the five proteins that had been identified by the screen of chromosome I. I performed Western blot

analysis for detecting the protein levels and the gTOW analysis for measuring plasmid copy number and calculated the fold change of the protein levels per gene copy. This analysis showed that the protein levels per gene copy were similar with the endogenous protein levels. Therefore, I conclude that dosage compensation was observed when considering the total protein levels and was captured by measuring the level of endogenous protein. Second, I verified dosage compensation of a subset of candidates using the GFP tag in order to examine the possibility that dosage compensation was observed due to the TAP tag. I used the same experimental setup with the analysis of endogenous TAP-tagged proteins (Figure 2.3A) and measured the levels of the dosage-compensated proteins Rbg1 and Mtw1 and the uncompensated protein Pop8. This experiments showed dosage compensation of Rbg1 and Mtw1 but not Pop8. Because this result is consistent with the observations obtained with the TAP tag, I conclude that dosage compensation is not a TAP-tag-mediated phenomenon.

Because a plasmid collection for the genome-wide gTOW analysis was prepared in a previous study [18], I used it and screened more than 50% (54 out of 96) of genes on *S. cerevisiae* chromosome I. Genome-wide collections of TAP- or GFP-tagged yeast strains are also available [33,37], so that the method developed in this study can be applied to a genome-wide screen. I believe that this challenge leads to a deeper understanding of robustness in gene expression and cellular systems. However, if trying to carry out this challenge, some modifications for the screening method are necessary in order to make it high-throughput because Western blotting for TAP-tagged proteins performed in the screen is low-throughput. Here, I propose three modifications for a better experimental-setup applicable for the genome-wide analysis of the dosage-compensated genes in *S. cerevisiae*. As a premise of the three approaches, it is necessary to prepare the GFP-tagged strain harboring pTOW40836 (Figure 2.2) or the same plasmid carrying a gene of interest. I call these strains “multicopy GFP-strains”. First,

measuring fluorescence intensity of GFP in the multicopy GFP-strains by flow cytometer. This enables rapid screening and provides distribution of the number of GFP positive cells, so that it is possible to check whether there is a heterogeneous population. If this analysis would observe a heterogeneous population, including cells with high and low GFP intensities (low and high degrees of dosage compensation, respectively), and the gTOW analysis would show lower and higher gene copy numbers in cells with high and low GFP intensities, it allows us to expect that the degree of dosage compensation relates to gene copy number. Second, measuring GFP intensity in the multicopy GFP-strains by a plate reader, which also enables rapid screening. Because this analysis provides time course data, if changes in GFP intensity during dosage compensation are clear, it allows us to expect that there is a mechanism affecting dosage compensation level. Third, fluorescence microscopic analysis of the multicopy GFP-strains using the CellProfiler program [38]. The CellProfiler is able to automatically quantify GFP intensity in each cell. A recent study quantified the abundance and localization of yeast proteome by fluorescence microscopic analysis including quantification using the CellProfiler [39]. This study also used machine learning technique in order to quantify the abundance of proteins localized to each organelle. If applying this approach to the screen of the dosage-compensated genes, it may be possible to investigate the relationship between dosage compensation and the abundance of correctly localized protein. If protein localization would not differ during dosage compensation, it suggests that dosage compensation decreases the amount of protein but keeps the amount of functional protein constant. As described here, all three approaches have a potential to provide new frontiers for the research on dosage compensation.

2.5 Table

Table 2.1. 54 genes tested in the screen of chromosome I.

#	Gene	#	Gene
1	*BDH2*	28	*FUN26*
2	*BDH1*	29	*CCR4*
3	*ECM1*	30	*FUN30*
4	*CNE1*	31	*PSK1*
5	*GPB2*	32	*TPD3*
6	*PEX22*	33	*NTG1*
7	*ACS1*	34	*CYS3*
8	*FLC2*	35	*SWC3*
9	*OAF1*	36	*MDM10*
10	*AIM2*	37	*SPO7*
11	*AIM1*	38	*FUN14*
12	YAL044W-A	39	*ERP2*
13	*GCV3*	40	*SSA1*
14	*PTA1*	41	*VPS8*
15	*CDC24*	42	*TFC3*
16	*CYC3*	43	*NUP60*
17	*CDC19*	44	*ERP1*
18	*RBG1*	45	*SWD1*
19	*FUN12*	46	*RFA1*
20	*MTW1*	47	YAR009C
21	*POP5*	48	*BUD14*
22	*GIP4*	49	*ADE1*
23	*MYO4*	50	*CDC15*
24	*SAW1*	51	YAR028W
25	*DRS2*	52	*PRM9*
26	*LTE1*	53	YAR064W
27	*PMT2*	54	*PHO11*

2.6 Figures

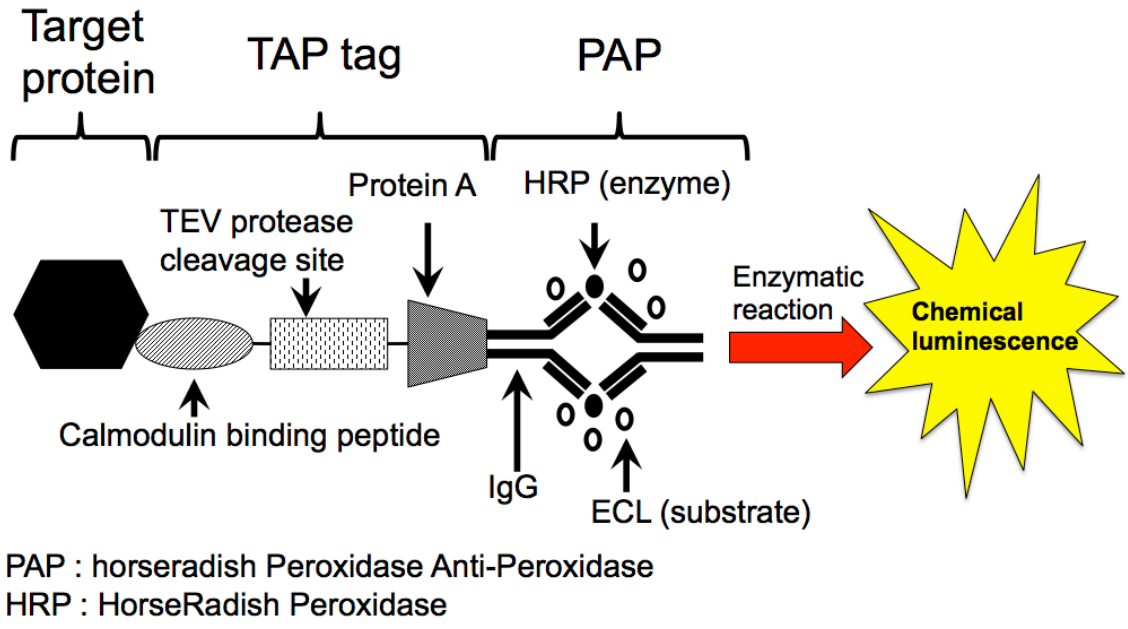

Figure 2.1. Overview of the detection of TAP-tagged protein by Western blotting with PAP.

Three components of the TAP tag: calmodulin binding peptide, tobacco etch virus (TEV) protease cleavage site, and Protein A. Peroxidase anti-peroxidase soluble complex (PAP) includes HRP and IgG, which binds to Protein A. HRP reacts with the substrate (the product is called ECL), and this enzymatic reaction induces chemical luminescence, so that TAP-tagged protein is detected by Western blotting with PAP.

A


M13_reverse 1..19
UP_primer 84..108
Target Gene Cloning Site 109..153
Down_primer 178..154
M13_forward 227..211
OSBI0870 295..276
OSBI0873 8274..8293
pBR322_origin 7410..8029
AmpR 6395..7255
pTOWug2-836
8401 bp
LEU2_cds 2349..1255
leu2d 2378..2378
URA3 6114..5158
EGFP 5156..4417

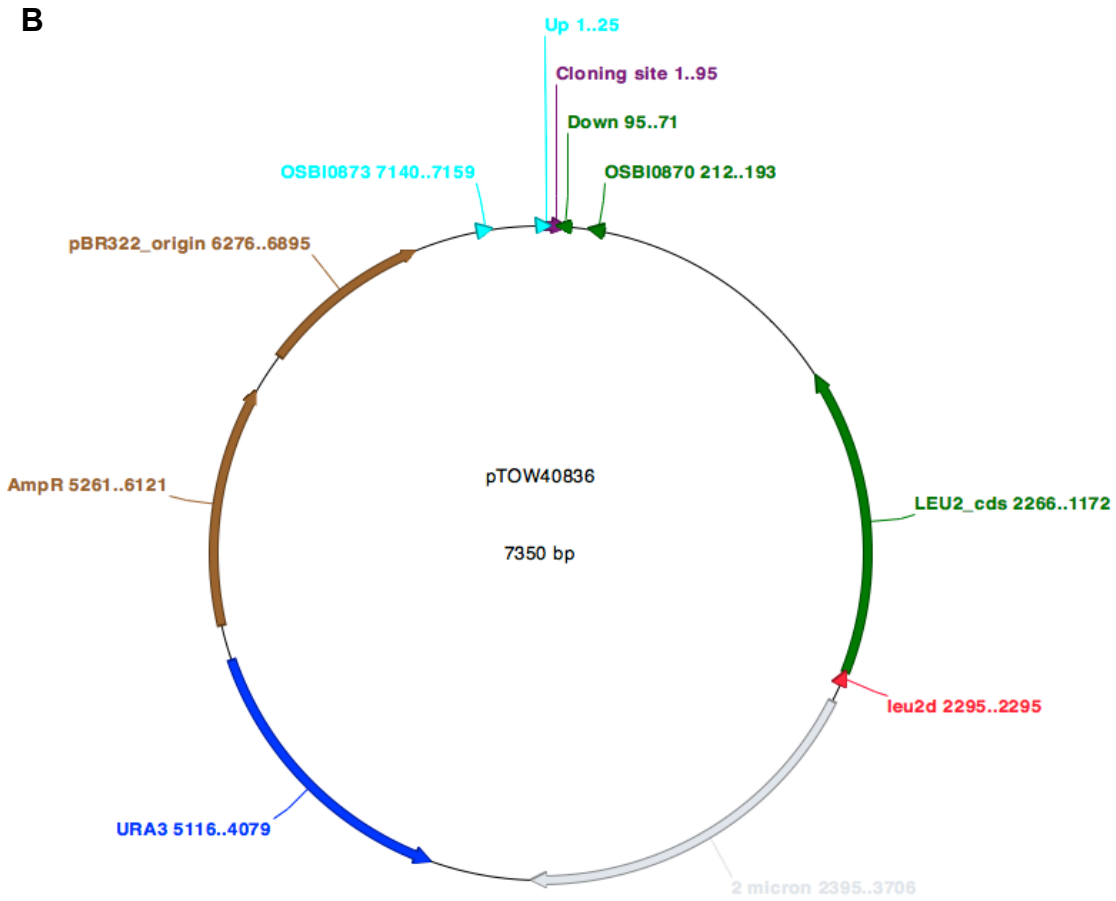

Figure 2.2. Maps of the multi-copy plasmid pTOWug2-836 and pTOW40836.

(**A**) The pTOWug2-836 plasmid contains *URA3* and *leu2-d* genes, which are used not only for selective markers but also for increasing the copy number of a target gene in the gTOW experiment as described above.

(**B**) The pTOW40836 plasmid is the same as pTOWug2-836 except that *EGFP* gene is not integrated into the 3´-end of *URA3*.

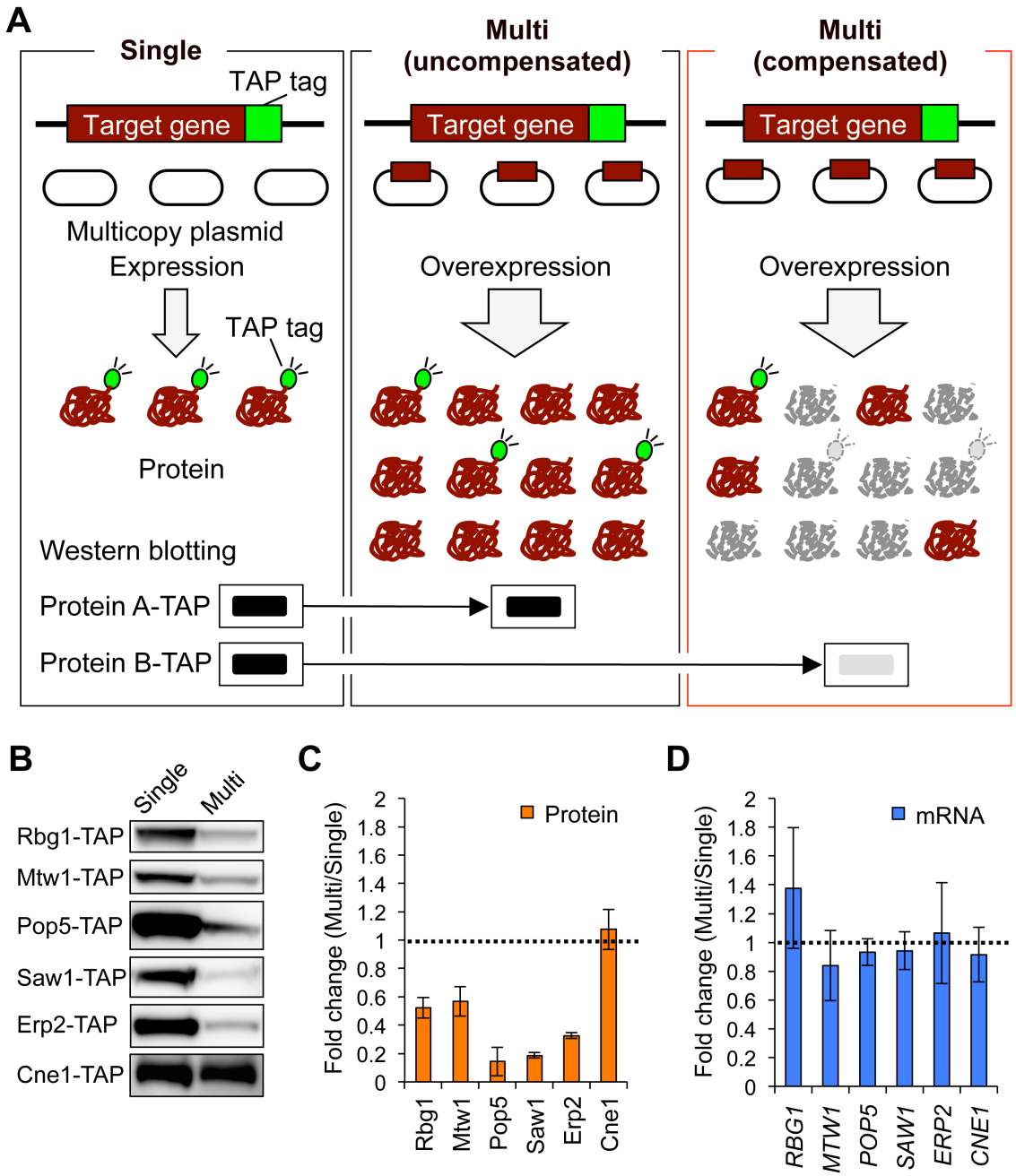

Figure 2.3. Identification of genes with dosage compensation.

(**A**) Schematic overview of the screening. Left panel (Single): TAP-tagged strain transformed with the empty vector. The native level of the target protein expressed only from the genomic copy is detected by Western blotting with PAP. Middle and right panels (Multi): TAP-tagged strain transformed with the multicopy plasmid carrying the target

gene without the TAP tag. If the level of TAP-tagged target protein is not reduced compared with that in the Single condition (middle panel), the target protein (Protein A) is not subjected to dosage compensation (uncompensated). If the level of TAP-tagged target protein is reduced compared with that in the Single condition (right panel), the target protein (Protein B) is subjected to dosage compensation (compensated). The cells carrying multicopy plasmid were grown in synthetic complete medium lacking uracil (SC–Ura).

(**B**) Western blots of proteins whose expressions are reduced upon an increase in their gene copy numbers. Cne1 is an example of the uncompensated proteins.

(**C, D**) Quantification of protein (**C**) and mRNA (**D**) expression levels of the identified genes. The mRNA level of each TAP-tagged target gene was measured by reverse transcriptase-PCR and normalized to *ACT1* mRNA levels. The average fold changes ± standard deviation (s.d.) from three biological replicates were calculated relative to the Single condition. Dashed line denotes the same expression level between the Multi and Single conditions.

Figure 2.4. Full results of the screening of the dosage-compensated genes.

More than 50% (54 out of 96) of genes on chromosome I were screened. Each rectangle includes the systematic name, standard name, and the result of Western blot (the Multi and Single conditions on the left and right, respectively). Rectangles with a pink line denote the dosage-compensated genes. A chromosome map was adopted and modified from the *Saccharomyces* Genome Database website [40].

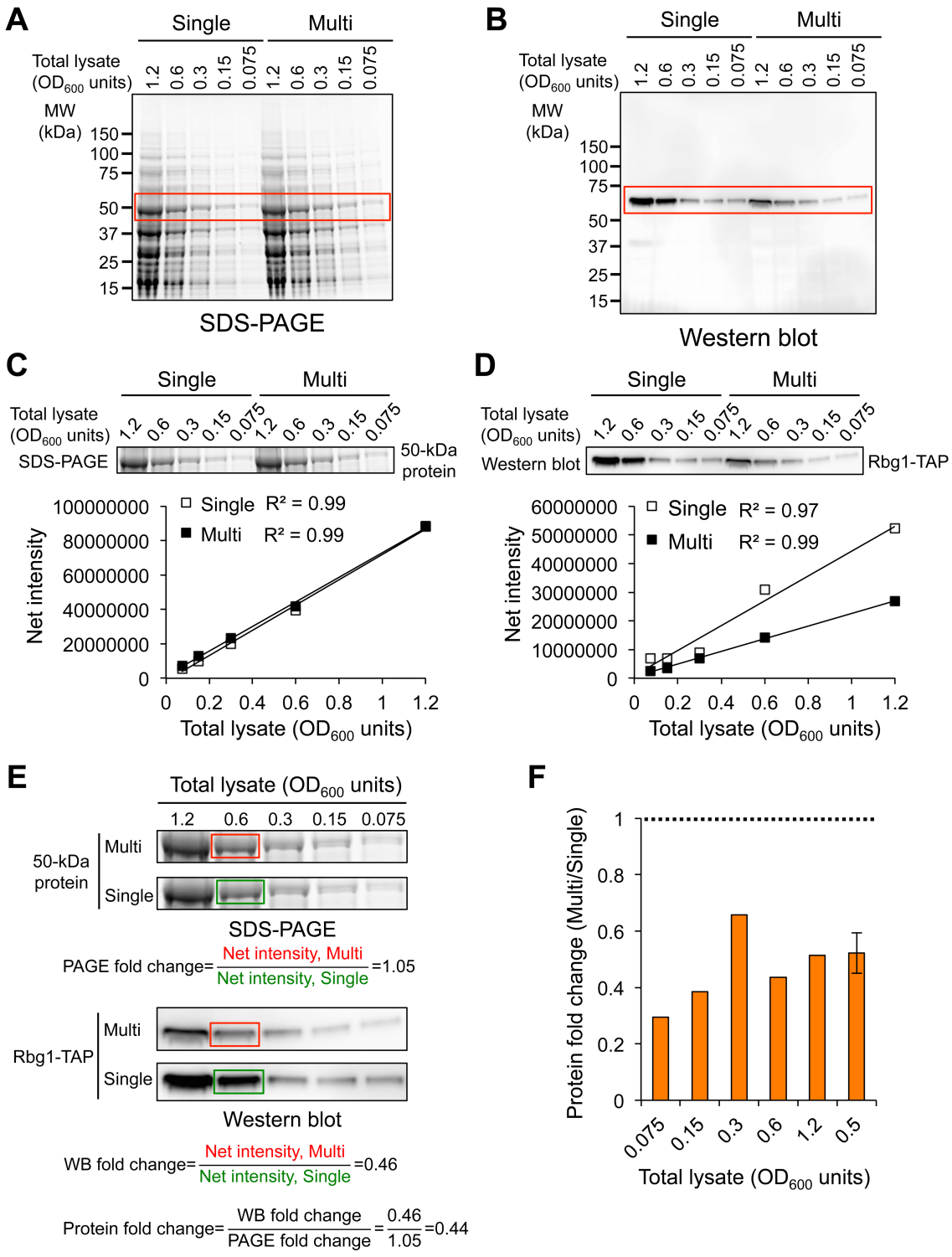

Figure 2.5. The linearity and accuracy of the protein quantification.

(**A**) SDS-PAGE of two-fold serially diluted cell lysate. The lysate prepared from cells

cultured in the Single or Multi conditions were loaded on the same gel. A red rectangle marks the area of a 50-kDa protein, corresponding to enolase, used as a loading control of Western blot analysis.

(**B**) Western blot of two-fold serially diluted cell lysate. The gel shown in Figure 2.5A was blotted onto PVDF membrane and Rbg1-TAP in the total lysate was detected by Western blot with PAP. A red rectangle marks the area of Rbg1-TAP.

(**C**) The area of a 50-kDa protein cropped from the gel shown in Figure 2.5A (upper panel). The signal intensity of each band was measured after background subtraction, and the net intensity was plotted on the y-axis (lower panel). The amount of lysate had a correlation coefficient (R^2) of 0.99 with the net intensity in both the Single and Multi conditions.

(**D**) The area of Rbg1-TAP cropped from the membrane shown in Figure 2.5B (upper panel). The net intensity of each band was measured after background subtraction, and the net intensity was plotted on the y-axis (lower panel). The amount of lysate had a correlation with the net intensity of Rbg1-TAP in the Single and Multi conditions (R^2 = 0.97 and 0.99, respectively).

(**E**) Quantification of fold change in Rbg1-TAP level between the Single and Multi conditions. The case of analyzing 0.6 OD_{600} units of cells is shown as an example. The net intensities of a 50-kDa protein and Rbg1-TAP from the Multi condition were divided by those from the Single condition to calculate the PAGE fold change and the WB fold change, respectively. Protein fold change was calculated by dividing the WB fold change by the PAGE fold change.

(**F**) The protein fold change calculated from the analysis of each OD_{600} units of cells. Only non-saturated signals were used for all the quantification analysis. Dashed line denotes the same expression level between the Multi and Single conditions. For comparison, the result of the Western blot analysis using 0.5 OD_{600} units of cells, the same

data shown in Figure 2.3C, is shown.

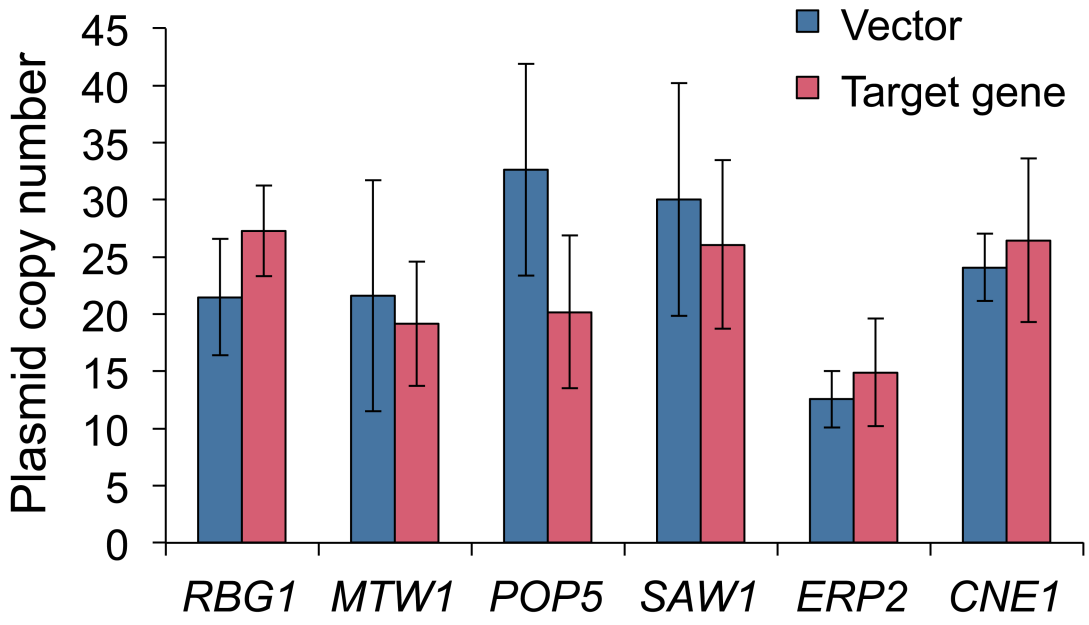

Figure 2.6. Gene copy number during dosage compensation.

Bar graph indicates the copy numbers of pTOWug2-836 (Vector) and the plasmid carrying each of the indicated genes in each TAP-tagged strain. The copy numbers were measured by the gTOW technique. The average copy numbers ± s.d. were calculated from four biological replicates.

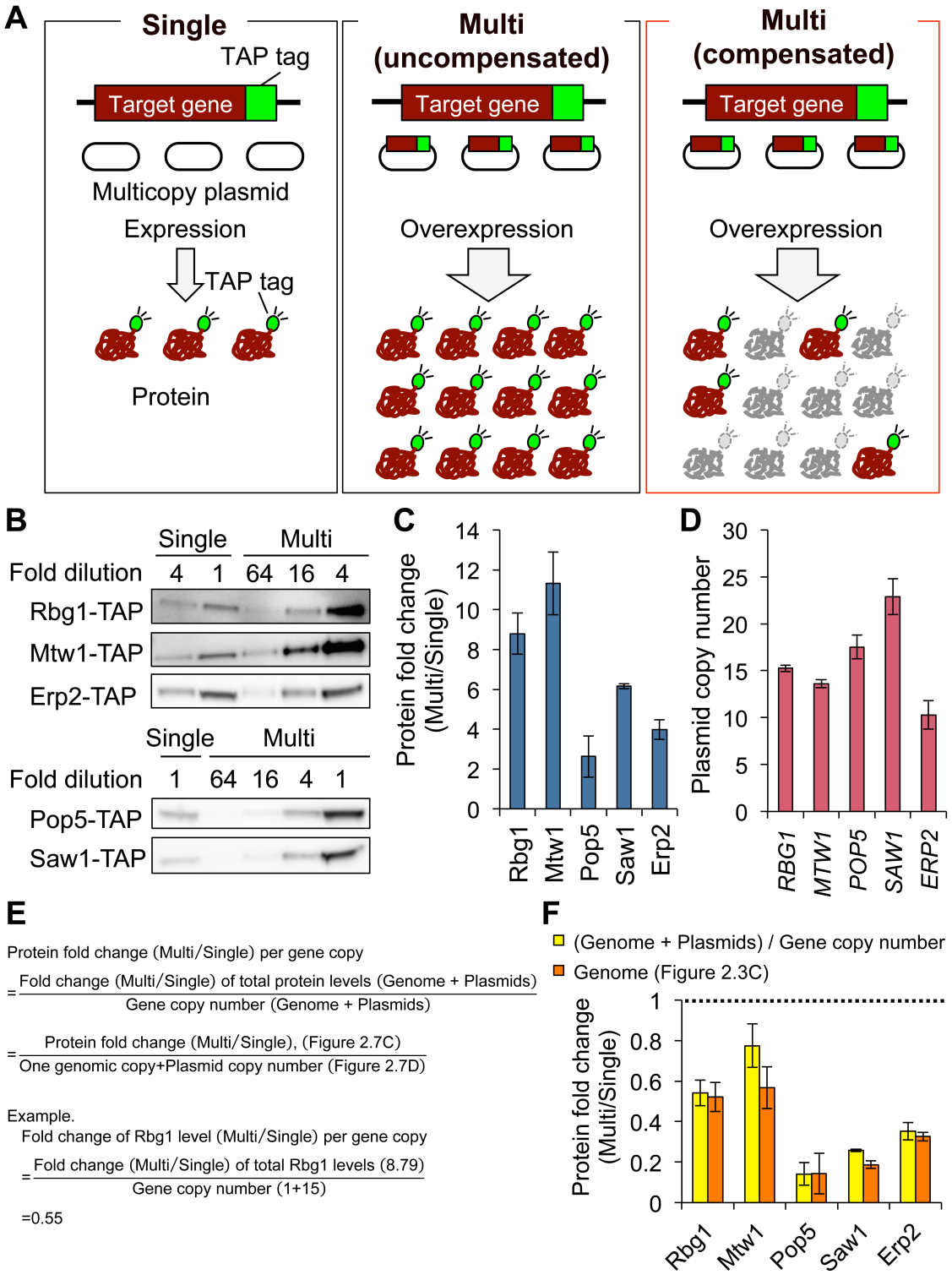

Figure 2.7. Observation of dosage compensation in the analysis of endogenous and exogenous protein levels.

(**A**) Schematic overview of the analysis of endogenous and exogenous proteins. Left panel (Single): TAP-tagged strain transformed with the empty vector. The native level of the target protein expressed only from the genomic copy is detected by Western blotting with PAP. Middle and right panels (Multi): TAP-tagged strain transformed with the multicopy plasmid carrying the target gene with the TAP tag. If the level of the TAP-tagged target protein per gene copy is not reduced compared with that in the Single condition (middle panel), the target protein is not subjected to dosage compensation. On the other hand, if the level of the TAP-tagged target protein per gene copy is reduced (right panel), the target protein is subjected to dosage compensation. The cells carrying a multicopy plasmid were grown in SC–Ura medium.

(**B**) Western blot with PAP for the indicated TAP-tagged proteins expressed from the genome and the multicopy plasmid.

(**C**) Quantification of the expression levels of the identified proteins. The average fold changes ± s.d. from three biological replicates were calculated relative to the Single condition. Protein levels at the same dilution in the Multi and Single conditions were used for the quantification.

(**D**) Bar graph indicates the copy number of pTOW40836 carrying each of the indicated genes with the TAP tag. The copy numbers were measured by the gTOW technique. The average copy numbers ± s.d. were calculated from more than three biological replicates.

(**E**) Quantification method of protein fold change per gene copy. The case of analyzing Rbg1 level is shown as an example. The fold change in Rbg1-TAP level between the Single and Multi conditions was divided by the *RBG1* copy number.

(**F**) Bar graph indicates the fold changes of the indicated proteins per gene copy. The average fold changes ± s.d. were calculated from three biological replicates. Dashed line denotes the same expression level between the Multi and Single conditions. For com-

parison, the result of Western blot analysis detecting the only endogenous target protein, the same data shown in Figure 2.3C, is shown.

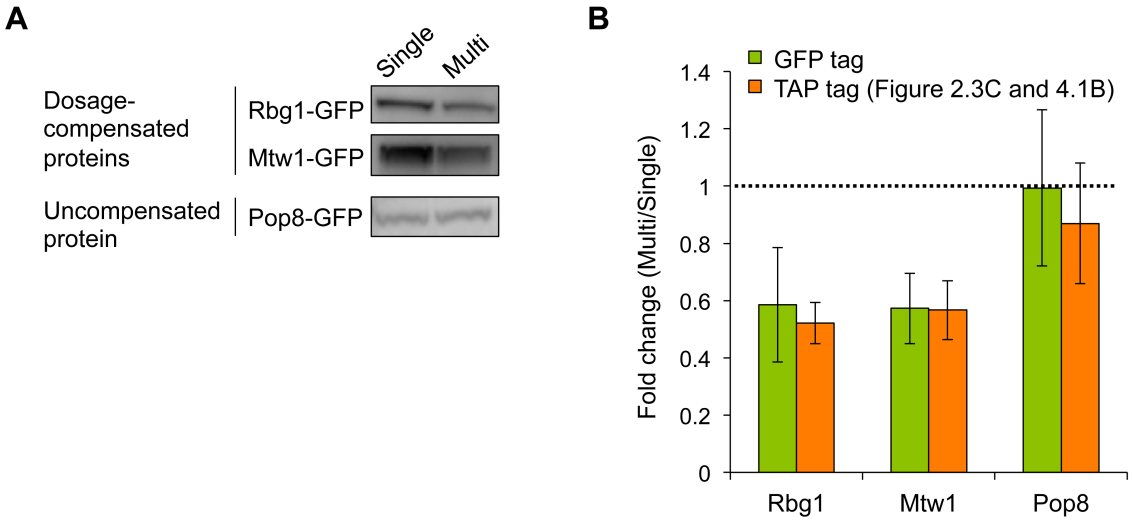

Figure 2.8. Observation of dosage compensation using the GFP tag.

(**A**) Western blot of the dosage-compensated proteins identified from the screen of chromosome I. GFP-tagged target proteins expressed from the genomic regions were detected with an anti-GFP antibody. Pop8 is an example of the uncompensated proteins. (**B**) Quantification of the expression levels of the indicated proteins. The average fold changes ± s.d. relative to the Single condition were calculated from three biological replicates. Dashed line denotes the same expression level between the Multi and Single conditions. For comparison, the results obtained using the TAP tag, the same data shown in Figure 2.3C and 4.1B, are shown.

Chapter 3

Mechanism of dosage compensation

3.1 Introduction

Since mRNA levels of the dosage-compensated genes did not differ upon an increase in their copy number, there are two possible mechanisms that underlie protein-level dosage compensation: translation- and proteolysis-mediated compensation (Figure 3.1). Thus, I examined the contributions of two major degradation pathways the ubiquitin–proteasome and the autophagy–lysosome systems to dosage compensation using mutant strains of each pathway. I also examined the involvement of reduced translational efficiency in the compensation mechanisms using the ribosome profiling technique.

The ubiquitin–proteasome system is a major degradation pathway conserved in a wide range of eukaryotic organisms, which selectively degrades ubiquitinated proteins as substrates. The 26S ubiquitin-dependent proteasome is a macromolecular complex and consists of one or two 19S regulatory particles and one 20S catalytic particle. Ubiquitin conjugated to a target protein is recognized by the 19S particles, and the ubiquitinated protein is unfolded and translocated into the 20S particle. Therefore, ubiquitination of the dosage-compensated protein is a direct evidence for the compensation by the ubiquitin–proteasome system. I used a mutant strain of the 19S particles to examine whether the degree of the compensation decreased in this mutant compared with that in wild-type cells and that ubiquitinated form of the dosage-compensated protein is accumulated in the 19S particles mutant.

The autophagy–lysosome system is one of the major pathways of protein degradation and is widely conserved in eukaryotic cells. This pathway is activated by various stress including starvation and is performed in the following three steps: (i)

formation of a characteristic intracellular structure autophagosome that surrounds a portion of cytosol, (ii) formation of autolysosome that is a fusion of the autophagosome and lysosome, and (iii) degradation of proteins in the autolysosome by many types of protease contained in lysosome. Because autophagy is performed in a non-selective manner and degrades a large amount of proteins at one time, autophagy is generally known as a bulk degradation system. Recent studies have shown some examples that autophagy selectively degrades specific organelle (e.g., nucleophagy, mitophagy, ER-phagy, pexophagy [41]) and proteins (e.g., Cue5-mediated degradation of ubiquitibated proteins [42], ribophagy for ribosome-specific degradation [43]). Activation of autophagy has been shown in aneuploid mammalian cells [44,45], which seems to confer tolerance to proteotoxicity due to aneuploidy-induced proteome imbalance. To verify autophagy-mediated dosage compensation, I used two autophagy mutants, *atg5Δ* and *pep4Δ* strains. Atg5 and Pep4 proteins play important roles in autophagosome formation and protein degradation in the autolysosome, respectively. The use of these mutants allowed examination of the contribution of each specific step in the progression of autophagy to dosage compensation. If autophagy is involved in the compensation mechanisms, the degree of the compensation should decrease.

In some disomic yeast strains, translational efficiency of the doubled number of genes is not altered [19,46]. This indicates that translational efficiency is not perturbed by an increased burden on cellular systems for protein homeostasis including the translation, folding, and degradation machineries. There may be no evidence of translation-mediated dosage compensation; however, in disomic yeast cells, there are the dosage-compensated proteins whose compensation levels are high even when treated with proteasome inhibitor MG-132 and autophagy inhibitor chloroquine [19]. Therefore, an investigation of the involvement of translational control in the compensation mechanisms is still needed in order to explain the reduction of protein level under genetic per-

turbations and better understand dosage compensation.

3.2 Materials and Methods

3.2.1 Strains

The W303-1B (*MATα ade2-1 his3-11,15 leu2-3,112 trp1-1 ura3-1 can1-100*) [47] and CMY765 (*MATα cim5-1 ura3-52 leu2Δ1 his3Δ200*) [48] strains were used for the analysis of the ubiquitin–proteasome system. The yeast strains BY4741, *atg5Δ* (*MATa atg5Δ*::*KanMX his3Δ1 leu2Δ0 met15Δ0 ura3Δ0*), and *pep4Δ* (*MATa pep4Δ*::*KanMX his3Δ1 leu2Δ0 met15Δ0 ura3Δ0*) were used for the analysis of the autophagy–lysosome system. BY4741 was used for ribosome profiling. These strains were transformed with empty vector pTOWug2-836 or the same vector carrying the gene of interest. Transformation of the yeast strains was performed by the lithium acetate method as described above.

3.2.2 Growth media and conditions

The transformants were grown at 30 °C except those that CMY765 was used as a host strain. CMY765 is a temperature-sensitive mutant, and 24 °C and 30 °C are permissive and semi-permissive temperature for its growth, respectively. The transformed cells of CMY765 strain were grown at 24 °C on SC–Ura plate, and then, the cells were inoculated in SC–Ura medium and grown at 30 °C.

3.2.3 TAP pull-down and Western blot analysis of ubiquitinated proteins

TAP-tagged strains carrying pTOW plasmid were grown at 30 °C in 100 mL of SC–Ura medium. The whole cells were harvested at log-phase and lysed with glass beads in 750 μL of lysis buffer [20 mM HEPES, 2 mM EDTA, 100 mM NaCl, 20% glycerol, 0.05% IGEPAL CA-630 (Sigma-Aldrich), Protease Inhibitor Cocktail, EDTA-Free (Thermo Scientific)] with 20 mM N-ethylmaleimide. The supernatant was immunoprecipitated using Dynabeads coated with pan-mouse IgG (Life Technologies), as described previ-

ously [49]. In short, the supernatant was incubated with 40 μL of Dynabeads in a Thermomixer Comfort (Eppendorf) at 21 °C for 2 h with shaking at 1300 rpm. The Dynabeads were washed one time with the lysis buffer and three times with the lysis buffer containing 150 mM NaCl and suspended in 16 μL of AcTEV buffer (Invitrogen) containing 1 mM DTT. Before TEV cleavage, for Western blot analysis of TAP-tagged protein, 2 μL of the suspension was removed and suspended in 10 μL of 2× NuPAGE LDS Sample Buffer and heated at 65 °C for 20 min. The remaining Dynabeads were then treated with 1 μL (10 units) of AcTEV protease (Invitrogen) in a Thermomixer Comfort at 4 °C for 16 h with shaking at 1300 rpm. The supernatant was subjected to Western blotting with polyclonal rabbit anti-ubiquitin antibody (DAKO) (1:500) as primary antibody and peroxidase-conjugated secondary antibody (Nichirei Biosciences). After TEV cleavage, the Dynabeads were suspended in 14 μL of 2× NuPAGE LDS Sample Buffer and heated at 65 °C for 20 min, and 2 μL of the extracts were mixed with 8 μL of 2× NuPAGE LDS Sample Buffer and analyzed by Western blotting with PAP. Detection of chemiluminescence was performed as described above.

3.2.4 Ribosome profiling

Yeast cells BY4741 expressing *POP5-TAP* from a single genomic locus and carrying pTOWug2-836 or pTOWug2-*POP5* were grown in 150 mL of SC–Ura at 30 °C with vigorous shaking. These cells were grown from an initial OD_{600} of approximately 0.2 to OD_{600} around 0.7, and the cells were then harvested by vacuum filtration. The cell pellet was immediately immersed in a 50 mL conical tube filled with liquid nitrogen and 2 mL of lysis buffer [10 mM Tris-HCl (pH 7.0), 10 mM Tris-HCl (pH 8.0), 150 mM NaCl, 5 mM $MgCl_2$, 1 mM DTT, 1% Triton X-100, 200 μg/mL CHX, 25 U/mL Turbo DNase (Invitrogen)] was dripped into the tube.

Extracts were prepared as previously described [29], except that the frozen

cells were pulverized with a mixer mill at 30 Hz. The total amount of RNA in the extracts was quantified using RiboGreen (Invitrogen), and then, 50 μg of total RNA was diluted to 300 μL with the lysis buffer. The sample was subjected to preparation of ribosome footprints according to a previously described method [50]. Briefly, total RNA was treated with RNase I (Epicentre), and then the ribosomal pellet was collected by sucrose cushion centrifugation. RNA was recovered from the pellet with TRIzol (Life Technologies) and purified with Direct-zol RNA MiniPrep (Zymo), followed by isopropanol precipitation. The resulting RNA was subjected to gel electrophoresis, and then, the 26–34-nucleotides regions were excised. The size-selected fragments were subjected to dephosphorylation with T4 PNK (New England Biolabs) and linker ligation with T4 Rnl2 (New England Biolabs). Ribosomal RNA (rRNA) was depleted from the sample using Ribo-Zero Magnetic Gold Kit for yeast (Epicentre). Reverse transcription was carried out with Protoscript II (New England Biolabs) on the rRNA-depleted sample. The reverse transcription product was then separated by gel electrophoresis, and the full-length product was excised.

The size-selected product was circularized with CircLigaseII (Epicentre). The circularized DNA was amplified by 6, 8, 10, 12, and 14 cycles of PCR with Phusion polymerase (New England Biolabs). The PCR products were loaded on gel, and the products of eight cycles were excised. The quality of the PCR product was assessed using Agilent 2200 TapeStation (Agilent Technologies). Deep sequencing (50 bp, single-end reads) was then performed on the Illumina HiSeq 4000 (Illumina). RNA sequencing (RNA-seq) libraries were generated using TruSeq Standard Total RNA Library Prep Kit (Illumina) from total RNA prepared as described above, and then, deep sequencing was performed in the same run with ribosome footprint sequencing.

The profiling analysis was performed according to the method previously described [50,51] with modifications for the analysis of budding yeast profiling. In short,

rRNA sequences were aligned to a set of budding yeast rRNA sequences, and then, non-rRNA reads were aligned to the budding yeast transcriptome. A-site offsets of ribosome footprints and mRNA fragments were estimated from 13 to 17 nucleotides for each read length of 26–30 nucleotides and 15 nucleotides for 22–51 nucleotides, respectively. The mapped reads excluding the first 15 codons and last 5 codons were counted based on the A-site offsets. DESeq was used to calculate fold change of RNA expression and translational efficiency [52]. Ribosome profiling and RNA-seq data analysis did not distinguish the reads from endogenous or exogenous *POP5* copies.

3.3 Results

3.3.1 Major contribution of the ubiquitin–proteasome system to dosage compensation

Given that dosage compensation is performed by post-transcriptional mechanisms (Figure 2.3D), the deceleration of protein synthesis and/or the acceleration of protein degradation should be the mechanisms of dosage compensation (Figure 3.1). I first examined the contribution of protein degradation by focusing on the ubiquitin–proteasome system, a major selective degradation pathway. I used CMY765 (*cim5-1*) strain as a proteasome-defective mutant [48] to test whether the compensation is not observed in this mutant. As shown in Figure 3.2A and 3.2B, the dosage compensations of Rbg1, Mtw1, and Erp2 were significantly weaker in *cim5-1* than in wild-type strain W303-1B (*CIM5*). The compensations of Pop5 and Saw1 also tended to be weaker in *cim5-1* mutant, although the difference was not statistically significant (Figure 3.3). The mRNA levels of these genes in *cim5-1* and *CIM5* cells did not differ (Figure 3.4).

To further verify the participation of the ubiquitin–proteasome system in dosage compensation, I examined the ubiquitination of the compensated proteins. The TAP-tagged proteins were immunoprecipitated with IgG-coated beads and cleaved with TEV protease, and the cleaved proteins were analyzed by Western blotting using anti-ubiquitin antibody (Figure 3.2C). Because the expression levels of the dosage-compensated proteins and the pull-down efficiency were different among the samples (Figure 3.2D), I normalized the ubiquitination level by dividing it by loading amount of immunoprecipitated proteins as described in Figure 3.2E. I compared the amount of the TAP-tagged proteins captured on the beads before and after TEV cleavage, which reflects the amount of immunoprecipitates analyzed by Western blotting for ubiquitinated proteins. This analysis showed a tendency to accumulate the greater amount of ubiquitinated proteins in *cim5-1* cells upon the Multi condition (Figure 3.2F).

These results strongly suggest that protein degradation by the ubiquitin–proteasome system is the main mechanism of dosage compensation.

3.3.2 The autophagy–lysosome system is not responsible for dosage compensation

Next, I examined protein levels of the dosage-compensated genes in *atg5Δ* or *pep4Δ* strains in which the TAP tag is integrated into the 3′-region of each target gene. *PEP4* encodes a protease contained in lysosomes, and a deletion mutant of this gene is often used as an autophagy-defective mutant as well as *atg5Δ* strain. I examined the levels of the five dosage-compensated proteins, identified by the screen of chromosome I, in the Multi and Single conditions by Western blot analysis with PAP. This analysis showed that for all genes tested, protein levels decreased in the Multi condition compared with those in the Single condition (Figure 3.5). In addition, the reduction of Rbg1 level was stronger in *atg5Δ* and *pep4Δ* strains than that in wild-type strain; fold changes are 0.41, 0.31, and 0.70 in *atg5Δ*, *pep4Δ*, and wild-type strains, respectively. These results indicate that dosage compensation was observed in autophagy mutants. Therefore, I conclude that the autophagy–lysosome system may not be involved in the compensation mechanisms.

3.3.3 Translational efficiency of *POP5* is not changed during dosage compensation

I also examined the contribution of translational control to dosage compensation. A high compensation level of Pop5 in *cim5-1* cells (Figure 3.2B) prompted me to measure the translational efficiency change upon an increase in *POP5* copy number. I performed ribosome profiling and RNA-seq and measured translation rate comparing between the Single and Multi conditions of Pop5 gene copy number. While a high copy number of *POP5* led to an increase in its mRNA expression (Figure 3.6A and 3.6C), the ribosome density per mRNA was not changed (Figure 3.6B and 3.6C). The RNA-seq analysis al-

so indicates that an increase in *POP5* copy number by the gTOW technique specifically increased its mRNA level and did not induce off-target effects on mRNA expression of the other genes. Therefore, I conclude that translational efficiency is not responsible for dosage compensation, at least in the case of Pop5. Residual proteasome activity in *cim5-1* mutant or alternative systems may specifically degrade Pop5 protein upon an increase in its gene copy number.

3.4 Discussion

Understanding the underlying mechanisms of dosage compensation does expand our understanding of cell robustness for buffering against genetic perturbations. I examined the involvement of the ubiquitin–proteasome system, the autophagy–lysosome system, and downregulation of translational efficiency in the compensation mechanisms. These analyses revealed that proteasomal degradation is the mechanism of dosage compensation (Figure 3.2). Although accumulation of ubiquitinated proteins has been found in disomic yeast strain [15], ubiquitination of the dosage-compensated proteins has not been shown. In this study, I obtained direct evidence for ubiquitination of the individual dosage-compensated proteins by performing immunoprecipitation of the dosage-compensated proteins (Figure 3.2C). On the other hand, the contribution of the autophagy–lysosome system and translational control to the compensation was not observed in the analysis of autophagy mutants and wild-type cells carrying high copy numbers of Pop5 gene, respectively. Taken together, the ubiquitin–proteasome system may be the main mechanism of dosage compensation. For the further study, identification of the E3 ubiquitin ligase responsible for dosage compensation may provide a deeper understanding of upstream process of ubiquitin-dependent dosage compensation. Previous study suggests that Tom1 is one of the E3 ubiquitin ligases that contributes to cope with gene overexpression from the observation that *tom1Δ* strain is sensitive to overexpression of histone H3 (Hht2) compared with wild-type strain [53]. Because there are large numbers of the E3 ligases in *S. cerevisiae*, systematic identification is preferable for further analysis needed for bridging a gap between an increase in gene copy number and ubiquitination of the dosage-compensated proteins.

Interestingly, in the analysis of autophagy, I observed higher reduction of Rbg1 and Pop5 levels in *atg5Δ* and *pep4Δ* strains than in wild-type strain. This might result from upregulation of proteasome activity induced by a defect in autophagy be-

cause there is a crosstalk between proteasome and autophagy [54,55]. Indeed, higher proteasome activity was observed in autophagy mutants [56]. Since degradation by the 26S proteasome may be the main mechanism of dosage compensation, this upregulation of proteasome activity may explain the lower levels of the dosage-compensated proteins in *atg5Δ* and *pep4Δ* strains. In other words, these data support that dosage compensation is performed through ubiquitin-dependent degradation.

As described above, I obtained no evidence of the involvement of autophagy in dosage compensation. A contribution of autophagy to the compensation has been expected in mammalian aneuploid cells because higher expression of autophagy-related proteins were observed [27,44]; however, it has not been observed in aneuploid yeast cells. This observation is thought to reflect differences in cell systems between mammalian and yeast cells. Further studies are needed to determine whether autophagy participates in dosage compensation and to elucidate the mechanisms behind that observation.

This study shows no evidence for a direct effect of translational efficiency to the compensation of Pop5 protein (Figure 3.6B and 3.6C). This result supports the robust translational efficiency of duplicated genes in aneuploid yeast strains [19,46]. However, it should be noted that an increase in a single gene to approximately 20 copies does not result in a decrease in ribosome occupancy for its mRNAs (Figure 2.6, 3.6B, and 3.6C). I speculate that translational efficiency is not responsible for dosage compensation and that translation is quite robust against genetic perturbations caused by an increase in gene copy number.

3.5 Figures

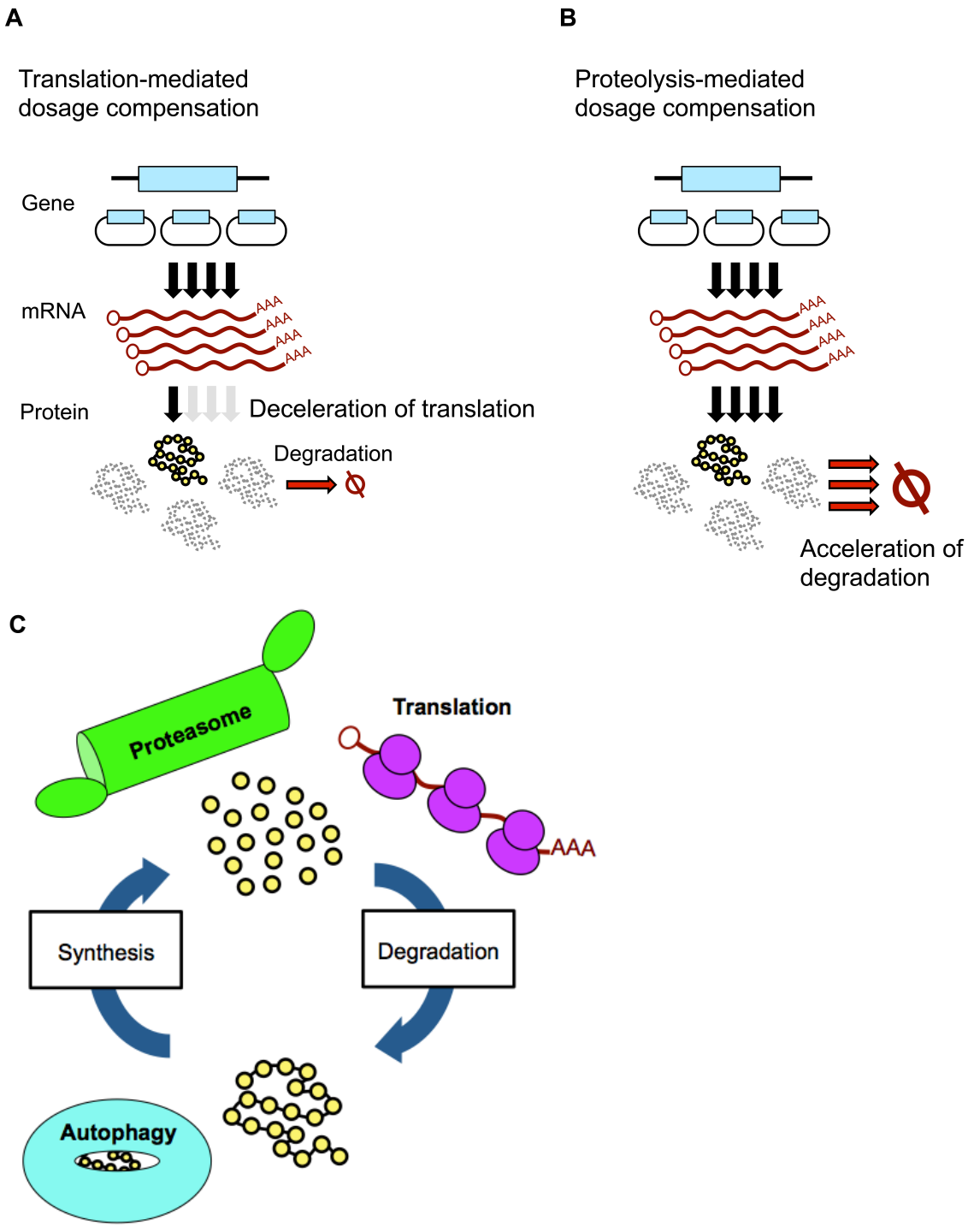

Figure 3.1. Possible mechanisms of dosage compensation.

(**A, B**) The abundance of mRNA and protein in a cell is a result of a balance between their synthesis and degradation. If a target gene is not subjected to protein-level dosage compensation, an increase in gene copy number results in a linear increase in mRNA and protein levels. A deceleration of translation (**A**) and an acceleration of degradation (**B**) can explain a nonlinear relationship between gene copy number and protein level via dosage compensation.

(**C**) Cells have two major protein degradation pathways, the ubiquitin–proteasome and the autophagy–lysosome systems, so that I examined the possibility of proteolysis-mediated dosage compensation by analyzing the contribution of each pathway to dosage compensation. I also examined the involvement of the translational control in the compensation mechanism.

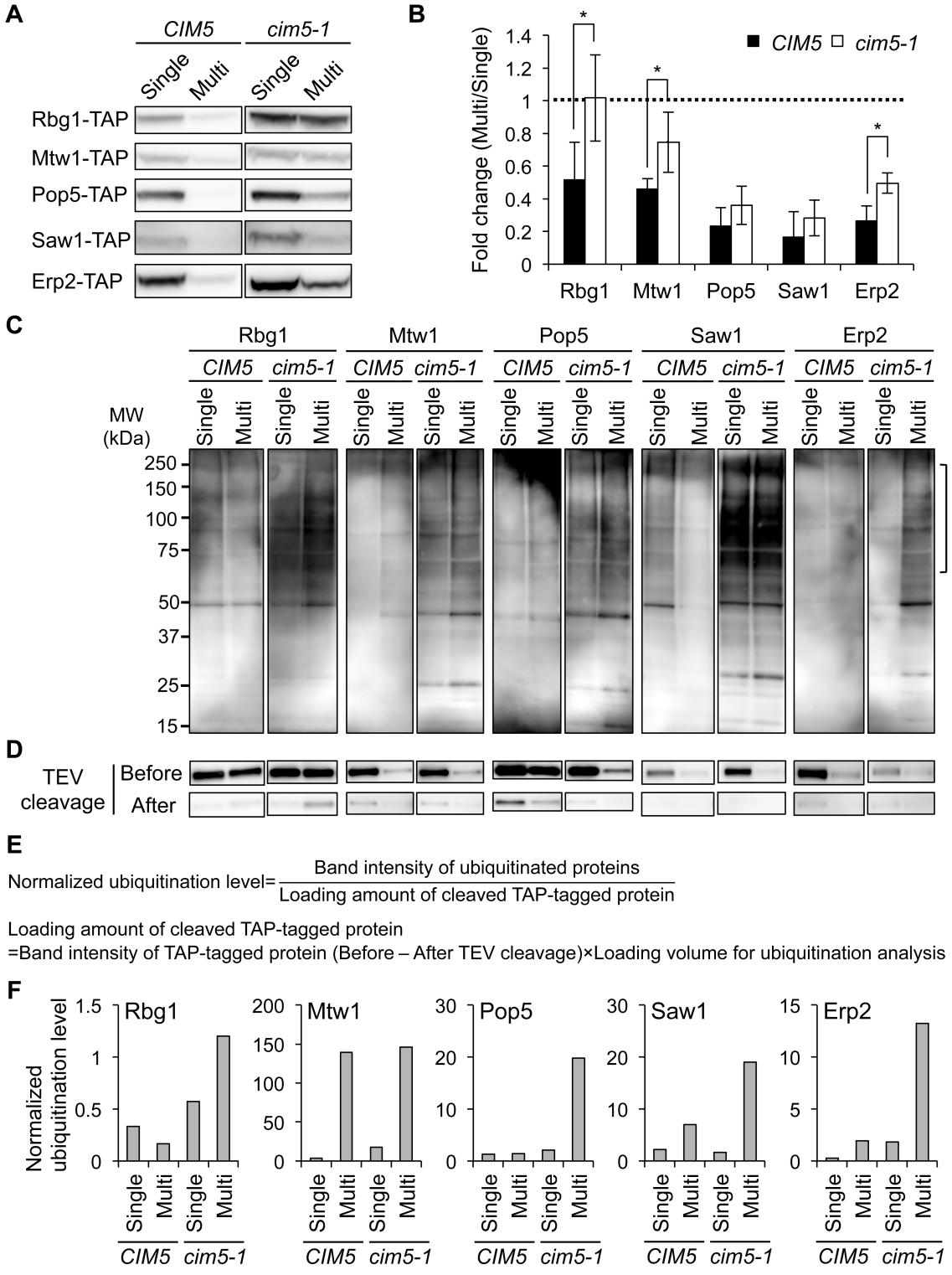

Figure 3.2. Major contribution of the ubiquitin–proteasome system to dosage compensation.

(**A**) Western blots showing the amount of the indicated proteins in *CIM5* (W303-1B) and *cim5-1* (CMY765) strains grown in SC–Ura medium. The TAP-tagged target proteins expressed from the genomic regions were detected with PAP.

(**B**) Quantification of the amount of the indicated proteins. The average fold changes ± s.d. from more than three biological replicates were calculated relative to the Single condition. Dashed line denotes the same expression level between the Multi and Single conditions. *P* values were determined by a one-tailed Mann Whitney *U* test (*$P < 0.05$).

(**C**) Ubiquitination of the dosage-compensated proteins. The TAP-tagged proteins expressed in the indicated conditions were immunoprecipitated with IgG-coated beads and cleaved with TEV protease, followed by Western blotting with anti-ubiquitin antibody. The bracket indicates poly-ubiquitinated species.

(**D**) Western blots of the dosage-compensated proteins captured on the beads. The TAP-tagged target proteins before and after TEV cleavage were detected with PAP. A combination of strain and condition of gene copy number in each lane is identical with Figure 3.2C.

(**E, F**) Quantification of the levels of ubiquitinated proteins. Band intensity of ubiquitinated proteins were normalized by dividing it by loading amount of the TAP-tagged proteins (**E**). Bar graph indicates the normalized ubiquitination level of each of the dosage-compensated proteins in *CIM5* and *cim5-1* cells under the Single and Multi conditions (**F**).

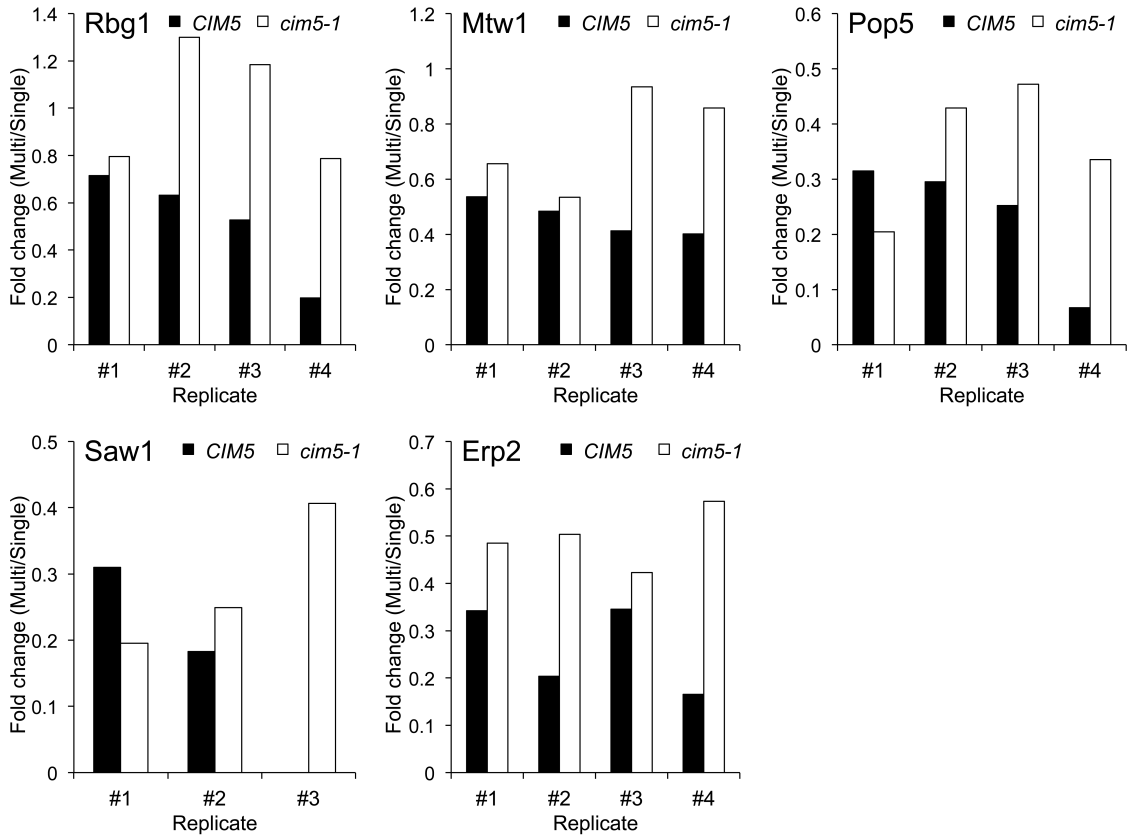

Figure 3.3. A tendency for reduced levels of dosage compensation in *cim5-1* strain. Bar graph indicates the fold change of each target protein. All data points of Figure 3.2B are shown. The fold change of Saw1 level in *CIM5* strain of replicate #3 was almost zero.

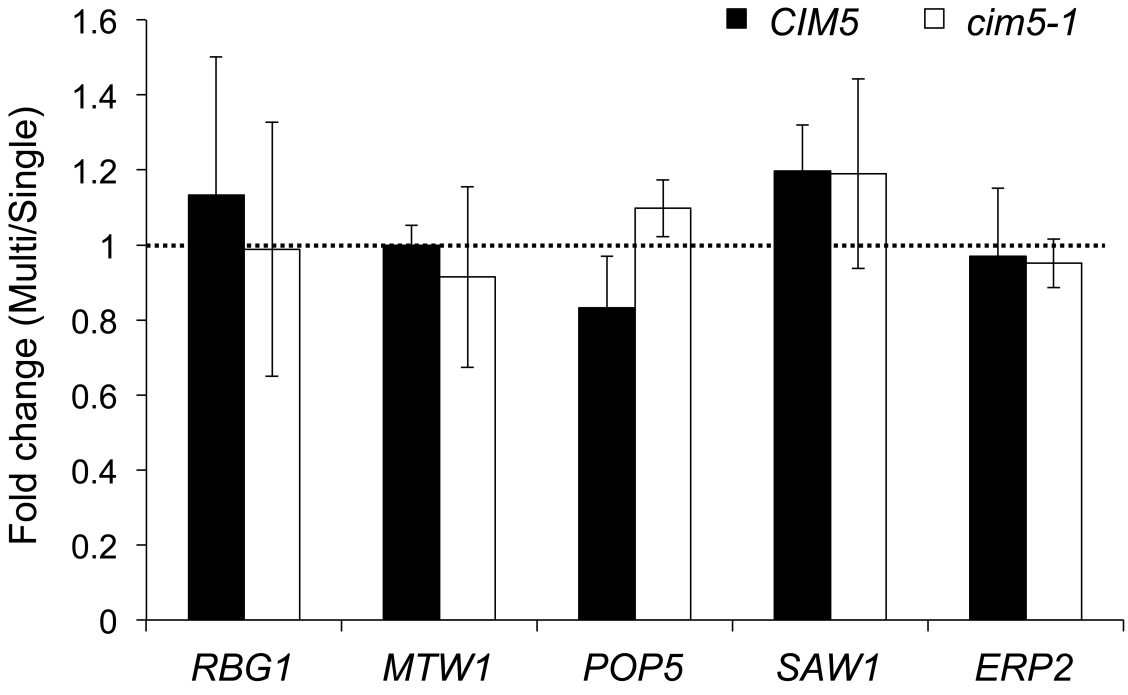

Figure 3.4. The mRNA levels of the dosage-compensated genes in *cim5-1* strain.

The *TAP* mRNA levels of the indicated genes in *CIM5* (W303-1B) and *cim5-1* (CMY765) strains grown in SC–Ura medium. The mRNA levels were measured by reverse transcriptase-PCR and normalized to *ACT1* mRNA levels. The average fold changes ± s.d. from three biological replicates were calculated relative to the Single condition. Dashed line denotes the same expression level between the Multi and Single conditions.

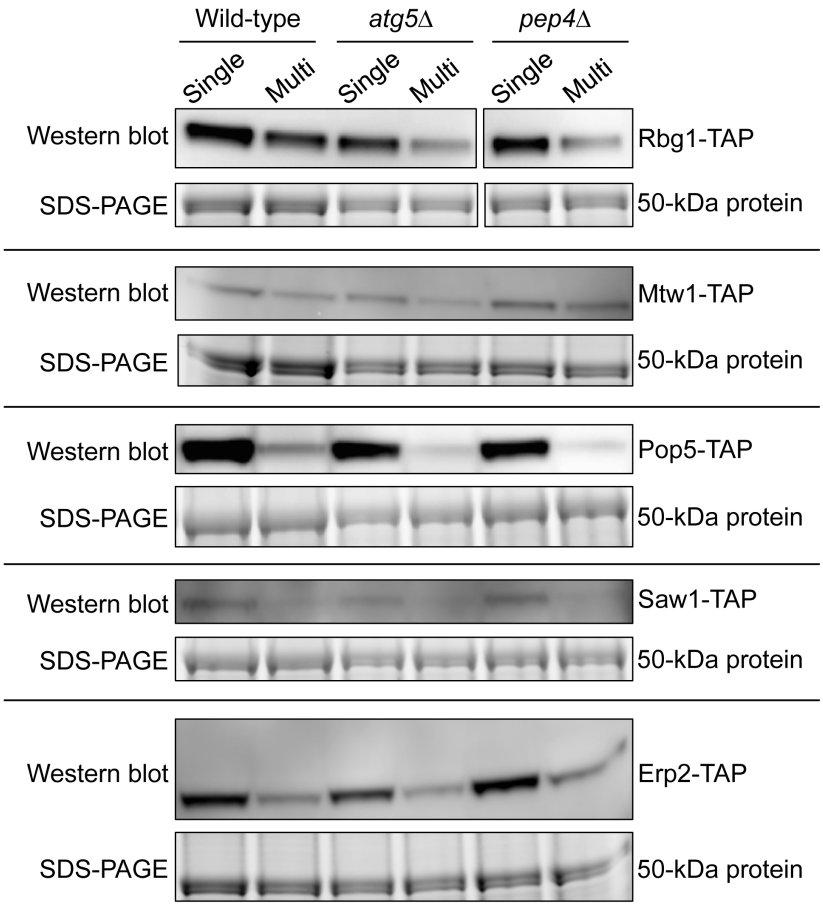

Figure 3.5. Dosage compensation is observed in autophagy mutants.

Western blot analysis of the indicated proteins in *atg5Δ* and *pep4Δ* strains grown in SC–Ura medium. The TAP-tagged target proteins expressed under the Single or Multi conditions were detected with PAP. A 50-kDa protein on SDS-PAGE is shown as a loading control.

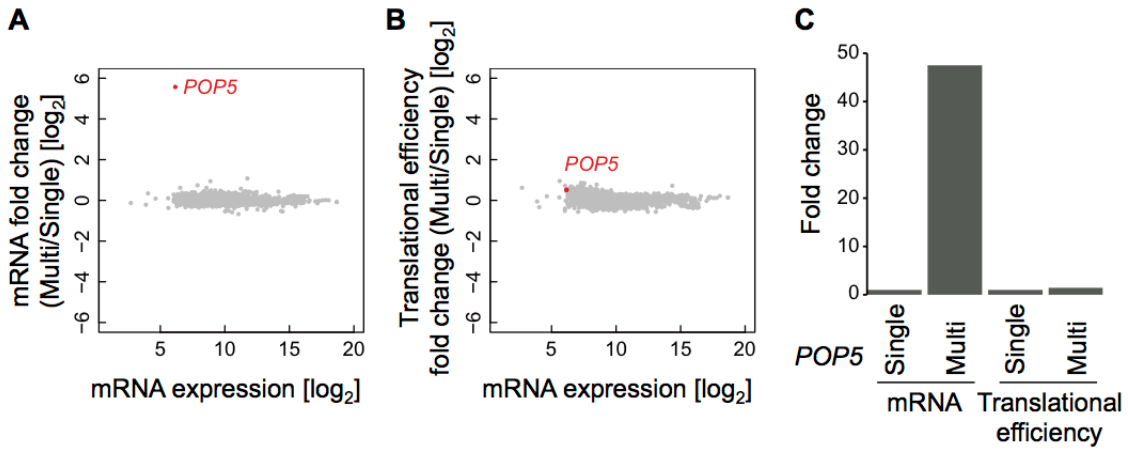

Figure 3.6. Translational efficiency of *POP5* is not changed during dosage compensation.

(**A, B**) Scatter plots showing the changes in mRNA levels (**A**) and the translational efficiency (**B**) of the genome in the Pop5-TAP strain carrying multicopy plasmid pTOWug2-*POP5* grown in SC–Ura medium. The X-axes indicate the mRNA level of each gene obtained by RNA-seq (mean counts in RNA-seq). The translational efficiency of each gene was calculated by dividing the ribosome density by the mRNA level. The mean fold changes relative to the Single condition were calculated from two biological replicates.

(**C**) Bar graph indicates the mRNA level and translational efficiency of *POP5* shown in Figure 3.6A and 3.6B.

Chapter 4

Biological role of post-translational dosage compensation

4.1 Introduction

The screen of chromosome I identified five dosage-compensated genes, and interestingly, all screened genes encode subunits of different complexes. As listed in Table 4.1, functional similarities were not found among these complexes. This result is in agreement with the previous findings that protein levels for duplicated genes encoding complex subunits tend to be reduced in aneuploid *S. cerevisiae* strains [19,25]. A similar observation was also reported in wild-type *Schizosaccharomyces pombe* carrying high copy numbers of subunit genes [35]. Furthermore, some ribosomal proteins were shown to be unstable and rapidly degraded if they are not assembled into a ribosomal complex [57]. Indeed, a very recent study has shown that overexpressed ribosomal proteins are subjected to protein-level dosage compensation through rapid degradation [58]. This study has also shown that overexpressed ribosomal proteins are not assembled into ribosomes, which strongly suggests that dosage compensation affects not only subunit levels but also complex levels. On the other hand, there is a previous study showing a general lack of dosage compensation [59]. This study used a series of diploid *S. cerevisiae* strains lacking one of the two alleles of each gene, and measured the protein level expressed from only one allele. More than 700 genes were tested with this experimental setup. This analysis showed that for at least 80% of the tested genes, their protein levels were close to 50% of those in wild-type strain and that for less than 5% of the ones, the protein levels were almost same as those measured in wild-type strain. This small subset of the compensated genes is not enriched in genes encoding subunits of protein complexes, and hence correlation between dosage compensation and complex subunits was

not found. As described above, it is open question whether complex subunits are predominant targets of protein-level dosage compensation. Therefore, in this study, I examined the relationship between complex subunits and dosage compensation using the same method that was developed for the screening of the dosage-compensated genes.

Genetic perturbations to the stoichiometry of complex subunits are strongly suggested to cause growth impairment due to an imbalance of subunit stoichiometry [10,13,18,26]. Given that complex subunits are predominantly targeted by dosage compensation, its biological role is expected to circumvent stoichiometric imbalance in multi-subunit complex. Experimental evidence for a regulation of complex levels by dosage compensation may provide a reasonable explanation for this hypothesis. In this study, I performed an analysis of not only subunit levels but also complex ones in order to examine whether dosage compensation contributes to robust formation of a protein complex.

4.2 Materials and Methods

4.2.1 Strains

The yeast strains BY4741 and *tma46Δ* (*MATa tma46Δ*::*KanMX his3Δ1 leu2Δ0 met15Δ0 ura3Δ0*) were used for the protein complex analysis. The TAP tag-encoding sequence was integrated into the 3´-region of each gene [33]. These strains were transformed with empty vector pTOWug2-836 or the same vector carrying the gene of interest. Transformation of the yeast strains was performed by the lithium acetate method as described above.

4.2.2 Growth media and conditions

The yeast strains BY4741 and *tma46Δ* without plasmid were grown at 30 °C in YPD medium. These strains with plasmid were grown at 30 °C in SC–Ura or SC–Leu–Ura media.

4.2.3 CHX chase assay

Yeast cells were grown to log-phase in SC–Ura, and 0.5 OD_{600} units were harvested for time point 0. Then, CHX was added to a final concentration of 200 μg/mL. Cells were harvested after 1, 2, 4, and 6 h of CHX treatment, followed by total protein extraction in 2× NuPAGE LDS Sample Buffer. The supernatant corresponding to 0.1 OD_{600} units was analyzed by Western blotting against the TAP tag as described above. The protein level at each time point was calculated as the intensity of Rbg1-TAP from Western blot divided by that of the 50-kDa protein, corresponding to enolase, from SDS-PAGE. The relative level was calculated by dividing the protein level at each time point by that at time point 0.

4.2.4 Native-PAGE analysis

Yeast cells were grown to log-phase in 6 mL of the appropriate medium and 5 OD_{600} units were harvested. The cells were washed with 1 mL of sterile water and lysed with glass beads in 250 μL of Digitonin buffer [1% Digitonin (Invitrogen), 1× NativePAGE Sample Buffer (Invitrogen), Protease Inhibitor Cocktail, EDTA-Free]. The supernatant corresponding to 0.2 OD_{600} units was mixed with NativePAGE 5% G-250 Sample Additive (Invitrogen) (final concentration 0.25%) and loaded on NativePAGE 4–16% Bis-Tris Gel (Invitrogen). The native gel electrophoresis was performed at room temperature with NativePAGE Running Buffer Kit (Invitrogen) according to the manufacturer's instructions. After electrophoresis, the gel was treated with SDS buffer [1× NuPAGE MOPS SDS Running Buffer (Invitrogen), 1% SDS] for 15 min. The gel was washed five times with 1× NuPAGE MOPS SDS Running Buffer, and then, blotted onto PVDF membrane using the iBlot system. After blotting, the membrane was washed with methanol for 5 min for three times, rinsed with PBST [1× PBS, 0.1% Tween 20] for three times, and washed in PBST for 10 min. The membrane was blocked with 4% skim milk in PBST for 1 h at room temperature before incubation with PAP (1:4000) in the same condition. Chemiluminescence was induced and detected as described above. The membrane was stained with CBB-R250 after immunoblotting.

4.3 Results

4.3.1 Complex subunits are predominant target of dosage compensation

Again, I note that all the five dosage-compensated genes identified by the chromosome I screen encode subunits of protein complexes as listed in Table 4.1. To investigate the relationship between dosage compensation and complex subunits, I analyzed other subunits of the same complexes. As shown in Figure 4.1, I found that six of seven subunits of the RNase MRP and nuclear RNase P complexes, *NSL1* in the MIND complex, and *EMP24* in the Erp2 complex were compensated at the protein level but not at the mRNA level. Quantification showed that the degree of compensation is very similar among the six subunits of the RNase MRP and nuclear RNase P complexes (Figure 4.1B). As listed in Table 4.2 and Figure 4.1D, I tested an additional 12 subunit genes and identified 7 dosage-compensated ones. This ratio is significantly higher than that identified in the initial screening (5 out of 54 genes) ($p < 10^{-9}$, chi-square test), although not all subunit genes are compensated. Thus, I speculated that dosage compensation predominantly targets complex subunits.

4.3.2 Model for maintaining subunit stoichiometry in the Rbg1–Tma46 heterodimer

As shown above, dosage compensation may be performed mainly through protein degradation and target predominantly complex subunits. Thus, I hypothesized that accelerated degradation of excess subunits that failed to construct a stable complex is the nature of dosage compensation. To test this, I focused on the Rbg1–Tma46 complex as a model complex. A working hypothesis is that when a subunit is overexpressed, there are two pools of subunit, the unstable pool that has not found a dimerization partner and the stable pool that is in a complex (Figure 4.2). The unstable pool is present but very small in the native condition where a large fraction of Rbg1 molecules are stable and a stoi-

chiometric balance between Rbg1 and Tma46 is in the steady state. In contrast, when Rbg1 is overexpressed, the unstable pool of Rbg1 is predominant. In the unstable pool, accelerated degradation of excess subunits should be observed.

4.3.3 Accelerated degradation of the dosage-compensated protein Rbg1

I first assessed the degradation of Rbg1 upon its overexpression by measuring the amount of Rbg1 after treating cells with a translational inhibitor, CHX. The CHX chase assay showed accelerated degradation of Rbg1 when its gene copy number was increased (Figure 4.3A and 4.3B), as I expected.

4.3.4 Bidirectional dosage compensation of Rbg1 in response to changes in gene dosage of its partner subunit Tma46

Next, I tested the effect of a loss and high copy number of *TMA46* on Rbg1 expression. In *tma46Δ* strain, the Rbg1 expression was reduced to less than 0.5-fold (Figure 4.3C and 4.4A). On the other hand, the amount of Rbg1 was increased more than 1.3-fold when the *TMA46* copy number was increased in wild-type cells (Figure 4.3D and 4.4B). These compensations are performed post-transcriptionally because the *RBG1* mRNA levels were not changed in these conditions (Figure 4.3C and 4.3D).

4.3.5 Dosage compensation through accelerated proteolysis buffers genetic perturbations to subunit stoichiometries at the complex level

To examine whether dosage compensation directly contributes to a higher or lower levels of the resulting complexes, the levels of the Rbg1–Tma46 complex were assessed by Native-PAGE followed by immunoblotting. This analysis confirmed that the complex was almost not detected in *tma46Δ* strain (Figure 4.3E). In wild-type cells, the levels of the TAP-tagged version of the Rbg1–Tma46 complex decreased and increased upon an

increase in *RBG1* and *TMA46* copy numbers, respectively (Figure 4.3F). These changes in the complex levels are consistent with the changes in the Rbg1 monomer levels in the same conditions.

The reduction of Rbg1 expression was recovered when *TMA46* copy number was increased in *tma46Δ* strain (Figure 4.5A). Quantification showed that the level of Rbg1 was significantly higher than that expressed in the same strain under the single-copy condition (Figure 4.5B and 4.6). The mRNA level of *RBG1* did not differ between them (Figure 4.5C). Furthermore, Native-PAGE analysis revealed that the level of the Rbg1–Tma46 complex also increased in *tma46Δ* strain upon an increase in *TMA46* copy number (Figure 4.5D). Therefore, I conclude that Rbg1 stability is modulated depending on the dosage balance against the partner molecule Tma46 and that dosage compensation affects not only subunit levels but also complex levels.

4.4 Discussion

Since all screened genes encode subunits of different complexes (Table 4.1), I examined whether other subunits of the complexes are subjected to dosage compensation. As a result, for 17 subunits included in these complexes, 70% (12 subunits) are subjected to dosage compensation (Figure 4.1 and Table 4.2). Given that the biological function of dosage compensation is to maintain subunit stoichiometry, these results explain the previous observation that cellular systems are very fragile to subunit gene overexpression [18]. This is also consistent with previous observations that the stoichiometric imbalance caused by aneuploidy strongly correlates with impaired cell growth [44,46]. Similarly, the findings from this study support a classical hypothesis called the balance hypothesis that predicts deleterious effects due to imbalanced subunit stoichiometry [26].

Although the screen of chromosome I suggests that the dosage-compensated genes encoding complex subunits constitute approximately 10% of the genome, subunit genes constitute 33% of the yeast genome. This suggests that there are other rules to distinguish between the compensated subunits and the uncompensated ones. Pop8 might be helpful for further characterization of the dosage compensation mechanism since the compensation level of only Pop8 differed from those of all other tested subunits of RNase MRP and nuclear RNase P complexes (Figure 4.1). Pop8 has the smallest number of interacting partners in these complexes, although the other subunits have at least two or more potential partners [60,61]. Therefore, Pop8 is suggested to be located at the peripheral region of these complexes. It is also known that only depletion of the Pop8 does not result in deleterious effects on RNase MRP function [61–66]. A similar observation in a different protein complex, oligosaccharyl transferase (OST), was recently reported [67]. The OST complex consists of nine subunits, including the functionally redundant Ost3 or Ost6 components, which are potentially the last subunit assembled into the complex. Overexpression of Ost3 or Ost6 does not lead to reduction of its pro-

tein level, whereas many of the other subunits show accelerated degradation upon their overexpression. Moreover, deletion of the Ost3 or Ost6 gene does not affect the protein level of the other subunits and results in only a small decrease in enzyme activity of the OST complex [67–69]. As listed above, characteristic features with similarities between Pop8 and Ost3 or Ost6 include the order of assembly, number of interactions, and responsibility for the function of each complex. Consideration of these features seems to provide other rules to determine the complex subunits predominantly regulated by dosage compensation.

As shown in Figure 4.3, the compensation of Rbg1 is performed in a stoichiometry-dependent manner between gene dosage of *RBG1* and *TMA46*. This bidirectional regulation of Rbg1 level may reflect changes in its degradation rate (Figure 4.3A and 4.3B). These results are analogous to bidirectional changes of Cog1 level upon overexpression of itself or its partner subunits: Cog2, Cog3, and Cog4 [70].

There are previous studies showing changes in the levels of the dosage-compensated subunits upon overexpression of themselves or their partner subunits. From these observations, dosage compensation has been postulated to contribute to the levels of subunits and also resulting complexes. However, no direct evidence has been reported for changes in the level of a complex by dosage compensation of its subunit. In this study, I performed Native-PAGE and immunoblotting to assess the levels of the dosage-compensated subunit Rbg1 and the Rbg1–Tma46 complex. This experiment indicates that dosage compensation of Rbg1 affects the levels of the Rbg1–Tma46 complex (Figure 4.3E and 4.3F) and that changes in the complex levels are consistent with those in the Rbg1 monomer levels. Therefore, I obtained direct experimental evidence that dosage compensation affects not only subunit levels but also complex levels.

4.5 Tables

Table 4.1. All screened genes encoding subunits of multi-protein complexes.

Gene	Annotation in *Saccharomyces* Genome Database
RBG1	Member of the DRG family of GTP-binding proteins; associates with translating ribosomes; interacts with Tma46p
MTW1	Essential component of the kinetochore complex; complex consists of Mtw1p including Nnf1p-Nsl1p-Dsn1p (MIND)
POP5	Subunit of RNase MRP and nuclear RNase P; RNase MRP cleaves pre-rRNA, while nuclear RNase P cleaves tRNA precursors
SAW1	5'- and 3'-flap DNA binding protein; complexes with Rad1p-Rad10p and stimulates its endonuclease activity
ERP2	Member of the p24 family involved in ER to Golgi transport; forms a heterotrimeric complex with Erp1p, Emp24p, and Erv25p

Table 4.2. Relationship between dosage compensation and complex subunits.

Gene	Complex	Subunit[a]	Tested subunit[b]	Compensated subunit	Reference
RBG1	Rbg1–Tma46	2	2	1	[71]
MTW1	Mtw1–Nnf1–Nsl1–Dsn1 (MIND)	4	3	2	[72]
POP5	RNase MRP and nuclear RNase P	10	7	6	[60]
SAW1	Saw1–Rad1–Rad10	3	1	1	[73]
ERP2	Erp2–Erp1–Emp24–Erv25	4	4	2	[74]

[a] This number includes only protein subunits, not RNA subunits.

[b] This number does not include subunits whose protein expression is not detected.

4.6 Figures

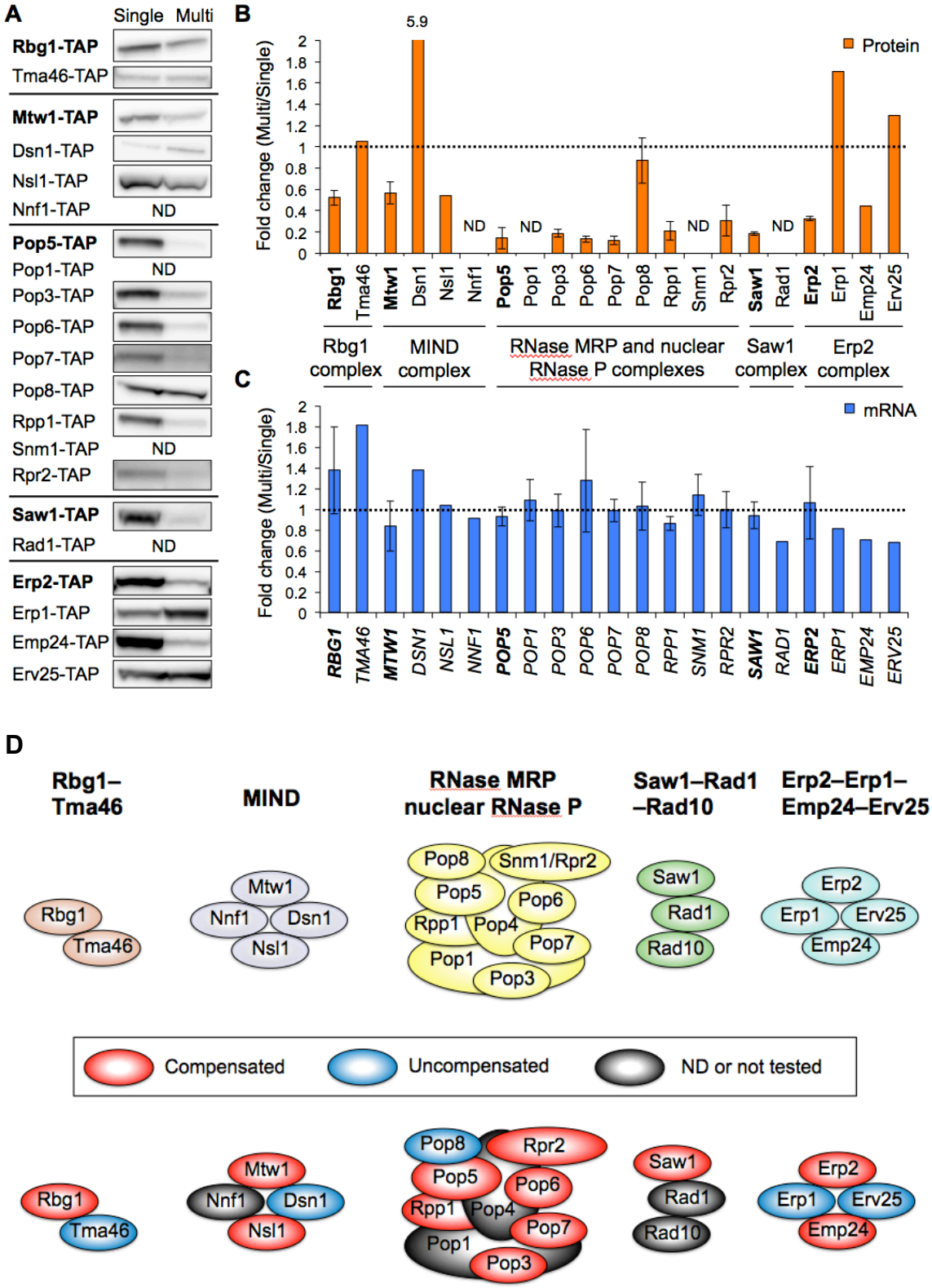
A
Single
Multi
Rbg1-TAP
Tma46-TAP
Mtw1-TAP
Dsn1-TAP
Nsl1-TAP
Nnf1-TAP
ND
Pop5-TAP
Pop1-TAP
ND
Pop3-TAP
Pop6-TAP
Pop7-TAP
Pop8-TAP
Rpp1-TAP
Snm1-TAP
ND
Rpr2-TAP
Saw1-TAP
Rad1-TAP
ND
Erp2-TAP
Erp1-TAP
Emp24-TAP
Erv25-TAP
B
5.9
Protein
Fold change (Multi/Single)
ND
Rbg1
Tma46
Mtw1
Dsn1
Nsl1
Nnf1
Pop5
Pop1
Pop3
Pop6
Pop7
Pop8
Rpp1
Snm1
Rpr2
Saw1
Rad1
Erp2
Erp1
Emp24
Erv25
Rbg1 complex
MIND complex
RNase MRP and nuclear RNase P complexes
Saw1 complex
Erp2 complex
C
mRNA
Fold change (Multi/Single)
RBG1
TMA46
MTW1
DSN1
NSL1
NNF1
POP5
POP1
POP3
POP6
POP7
POP8
RPP1
SNM1
RPR2
SAW1
RAD1
ERP2
ERP1
EMP24
ERV25
D
Rbg1–Tma46
MIND
RNase MRP nuclear RNase P
Saw1–Rad1–Rad10
Erp2–Erp1–Emp24–Erv25
Rbg1
Tma46
Mtw1
Nnf1
Dsn1
Nsl1
Pop8
Snm1/Rpr2
Pop5
Pop6
Rpp1
Pop4
Pop7
Pop1
Pop3
Saw1
Rad1
Rad10
Erp2
Erp1
Erv25
Emp24
Compensated
Uncompensated
ND or not tested

Figure 4.1. Complex subunits tend to be subjected to dosage compensation.

(**A**) Western blots of subunits composed of the five complexes. The experiments were performed using the same method with the screening. TAP-tagged target proteins expressed from the genomic regions were detected with PAP. The dosage-compensated proteins identified from the screening are shown in bold letters.

(**B**) Quantification of protein expressions of the subunit genes.

(**C**) Quantification of mRNA expressions of the subunit genes. The mRNA level of each TAP-tagged target gene was measured as described above. Dashed line denotes the same expression level between the Multi and Single conditions. The RNase MRP and nuclear RNase P subunit genes were analyzed in three biological replicates, and the average fold changes ± s.d. were calculated relative to the Single condition. ND: not detected.

(**D**) An overview of the analysis of the five complexes and the results shown in Figure 4.1A and 4.1B. For 17 subunit genes tested, 12 were subjected to dosage compensation.

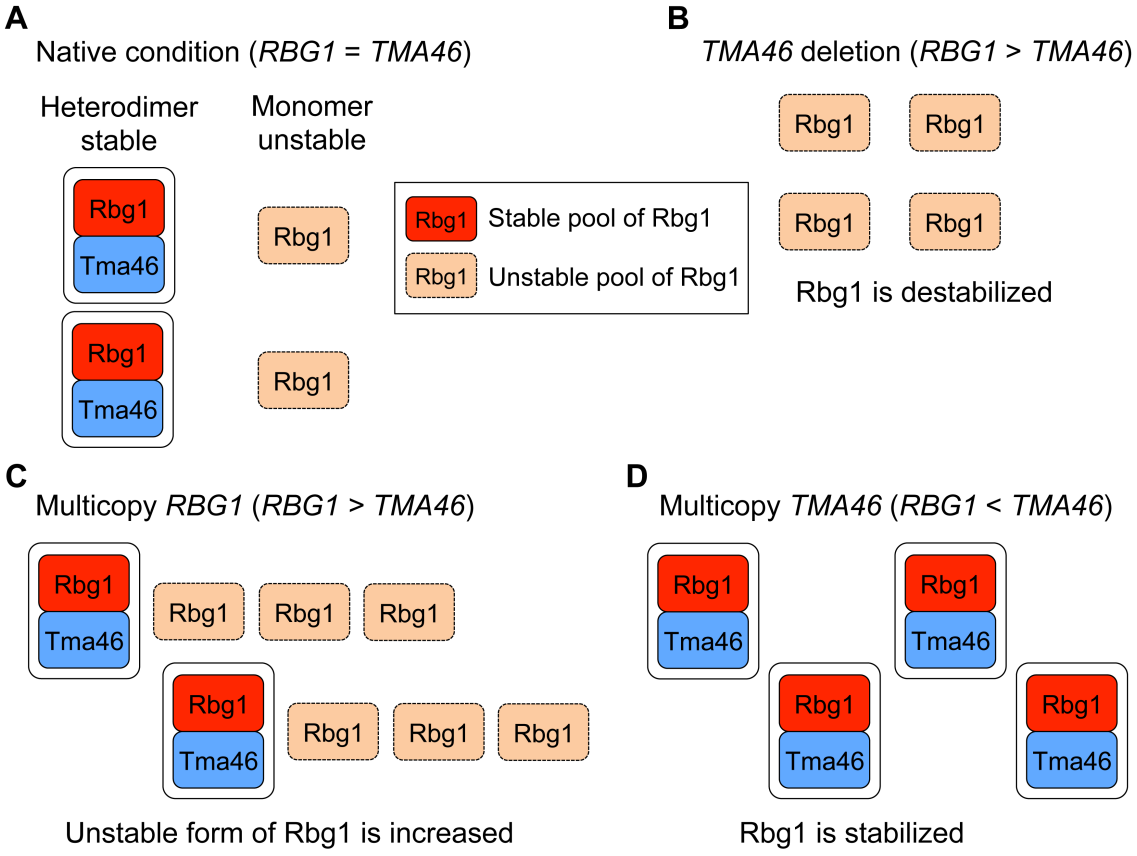

Figure 4.2. Model for maintaining subunit stoichiometry in the Rbg1–Tma46 heterodimer.

(**A**) Under native conditions, monomeric Rbg1 becomes more stable when it forms a complex with Tma46.

(**B**) Upon deletion of *TMA46*, Rbg1 is destabilized due to a loss of the partner subunit and rapidly degraded. The unstable pool of Rbg1 is predominant in this condition.

(**C**) Upon multicopy expression of Rbg1, the level of the unstable form of Rbg1 is increased, which is targeted for rapid degradation. The unstable pool of Rbg1 is predominant in this condition.

(**D**) Upon multicopy expression of Tma46, potentially degraded Rbg1 is stabilized by forming the Rbg1–Tma46 complex with an excess of Tma46. The stable pool of Rbg1 is predominant in this condition.

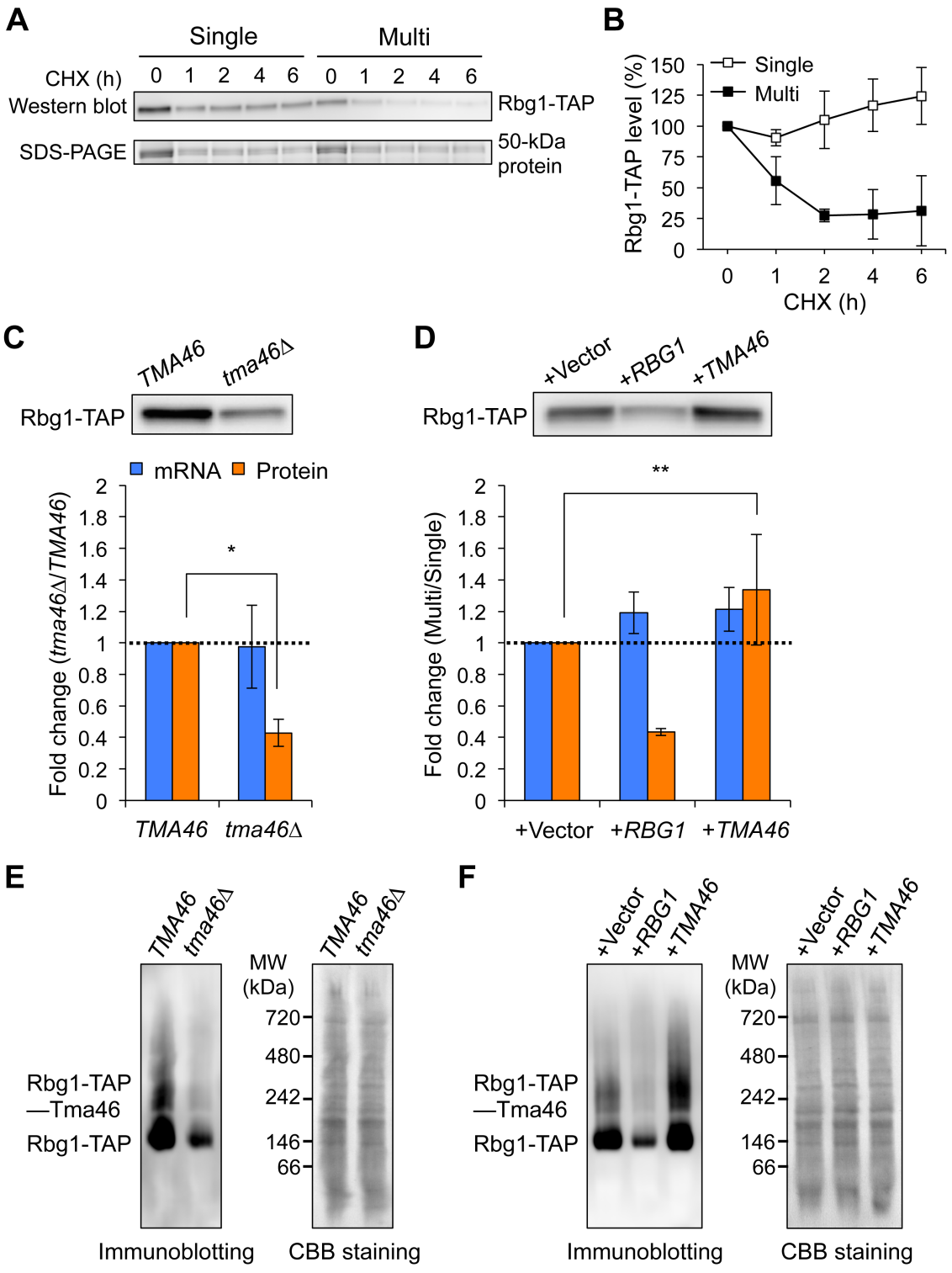

Figure 4.3. Dosage compensation through accelerated proteolysis buffers genetic perturbations to subunit stoichiometries at the complex level.

(**A**) Rbg1-TAP expressed in the Single and Multi conditions was detected by Western blotting with PAP after CHX treatment. A 50-kDa protein, corresponding to enolase, is used as a loading control.

(**B**) Quantification of the degradation of Rbg1-TAP. Percentage of the Rbg1-TAP level at each time point relative to the time point 0 is shown. The average expression levels ± s.d. were calculated from three biological replicates.

(**C**) The effect of *TMA46* deletion on Rbg1 expression. Rbg1-TAP expressed in wild-type and *tma46Δ* cells grown in YPD medium was detected by Western blotting with PAP (upper panel), and the fold changes were calculated (lower panel). The mRNA levels were measured as described above. The average fold changes ± s.d. from three biological replicates were calculated relative to the wild-type strain.

(**D**) The effect of multicopy *TMA46* on Rbg1 expression. Rbg1-TAP expressed under the Single (+Vector) and Multi (+*RBG1*: multicopy of *RBG1*, +*TMA46*: multicopy of *TMA46*) conditions were detected by Western blotting with PAP (upper panel), and the fold changes were calculated (lower panel). The mRNA levels were measured as described above. These cells were grown in SC–Leu–Ura to increase the plasmid copy number. The average fold changes ± s.d. of mRNA and protein levels relative to the Single condition were calculated from three and six biological replicates, respectively. Dashed line denotes the same expression level between the Multi and Single conditions. Statistical significance was determined by a one-tailed Mann Whitney *U* test (**P* = 0.05, ***P* < 0.03).

(**E, F**) The effect of *TMA46* deletion (**E**) and multicopy of *RBG1* or *TMA46* (**F**) on the levels of the Rbg1–Tma46 complex. The wild-type and *tma46Δ* cells without the plasmids and wild-type cells with the plasmids were grown in YPD and SC–Ura media, respectively. Rbg1-TAP and Rbg1-TAP–Tma46 expressed in these cells were detected by Native-PAGE followed by immunoblotting with PAP. Left: immunoblotting with PAP.

Right: total protein blotted onto the membrane and stained with CBB R250. A representative blot from two biological replicates is shown.

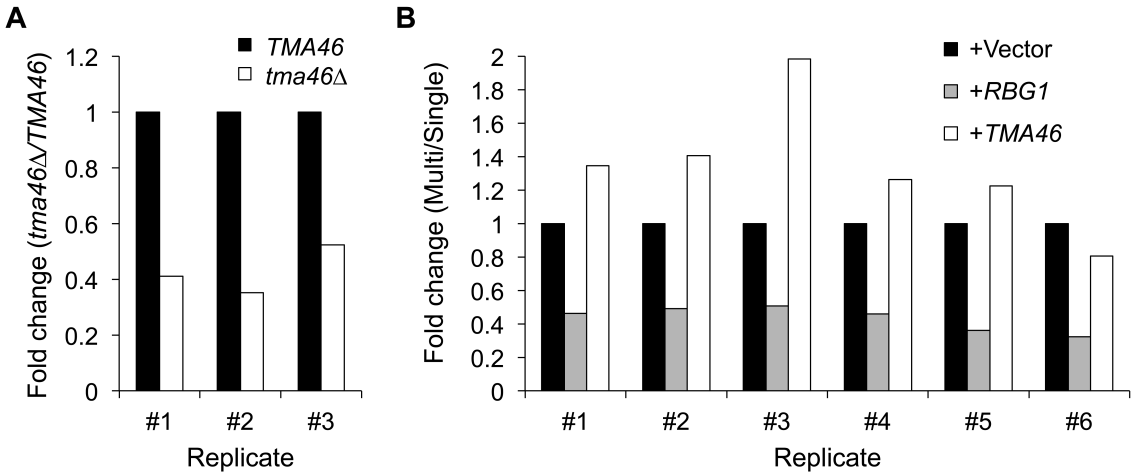

Figure 4.4. Bidirectional changes in Rbg1 level in response to *TMA46* copy number.

(**A**) The effect of *TMA46* deletion on Rbg1 expression. Rbg1-TAP expressed in wild-type and *tma46Δ* cells grown in YPD medium was detected by Western blotting with PAP, and the fold changes were calculated relative to the wild-type strain. All data points of Figure 4.3C are shown.

(**B**) The effect of multicopy *TMA46* on Rbg1 expression. Rbg1-TAP expressed under the Single (+Vector) and Multi (+*RBG1*: multicopy of *RBG1*, +*TMA46*: multicopy of *TMA46*) conditions were detected by Western blotting with PAP, and the fold changes were calculated relative to the Single condition. All data points of Figure 4.3D are shown.

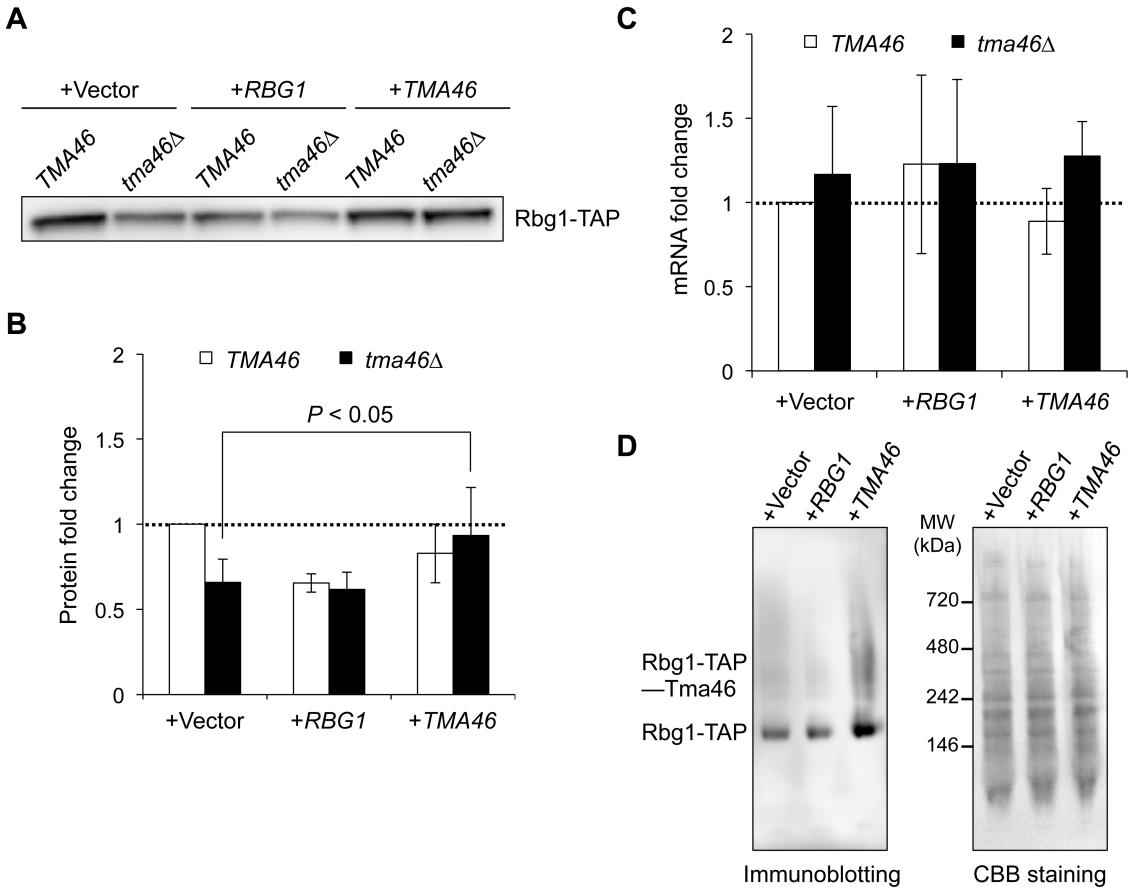

Figure 4.5. Multicopy of *TMA46* leads to an increase in the level of Rbg1 monomer and the Rbg1–Tma46 complex in *tma46Δ* strain.

(**A**) The effect of high copy *TMA46* on Rbg1 expression in *tma46Δ* strain. Rbg1-TAP expressed under the Single (+Vector) and Multi (+*RBG1*: multicopy of *RBG1*, +*TMA46*: multicopy of *TMA46*) conditions in wild-type and *tma46Δ* cells grown in SC–Ura medium were detected by Western blotting with PAP.

(**B**) Quantification of the data shown in Figure 4.5A. The fold change was calculated relative to the expression level in wild-type cells under the Single condition. Bar graphs show the average fold changes ± s.d. from five biological replicates. *P* value was determined by a one-tailed Mann Whitney *U* test. Dashed line denotes the expression level in wild-type cells under the Single condition.

(**C**) The mRNA levels of *RBG1* in each of the indicated conditions were measured as described above. The average fold changes ± s.d. were calculated from five biological replicates.

(**D**) Rbg1-TAP and Rbg1-TAP–Tma46 expressed in *tma46Δ* cells under the indicated conditions were detected by Native-PAGE followed by immunoblotting with PAP. Left: immunoblotting with PAP. Right: total protein blotted onto the membrane and stained with CBB R250. A representative blot from two biological replicates is shown.

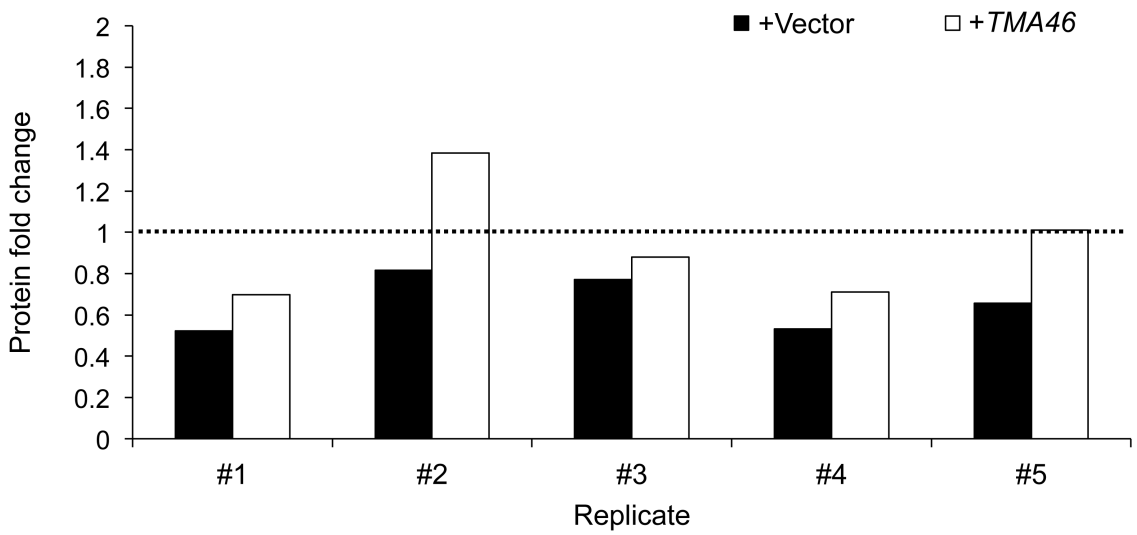

Figure 4.6. A significant tendency for the increased level of Rbg1 in *tma46Δ* strain carrying high copy numbers of *TMA46*.

The effect of high copy *TMA46* on Rbg1 expression in *tma46Δ* strain. Bar graphs show the level of Rbg1-TAP expressed under the Single (+Vector) and Multi (+*TMA46*: multicopy of *TMA46*) conditions in *tma46Δ* cells. All data points of Figure 4.5B are shown.

Chapter 5

General discussion

5.1 Post-translational dosage compensation regulates gene expression level at the final step of gene expression

This study extends our understanding of the rescue mechanism for perturbations causing the breakdown of biological systems. This study demonstrates that protein-level dosage compensation is responsible for robust expression of subunit genes under genetic perturbations. Correction of the subunit levels is performed at the final step in gene expression by protein degradation rather than earlier steps, mRNA transcription/degradation or translation. These results suggest that dosage compensation at the post-translational level is a critical step to mask the fragility caused by an increase in gene copy number. Furthermore, these findings in the context of systems biology provide a new foundation for the robustness of cellular systems.

5.2 The differences between the analysis of aneuploid cells and the gTOW analysis

The robustness in cellular systems to gene copy number changes has been investigated mainly using two approaches: generating aneuploidy of specific chromosomes [19,44] and introducing a plasmid carrying an individual target gene [18]. The generation of aneuploid cells containing one extra chromosome doubles the number of genes in the additional chromosome. Several recent studies using aneuploid yeast and mammalian cells have revealed fragility of cellular systems against gene copy number increase in a genome-wide manner [19,44]. The use of a multicopy plasmid carrying an individual target gene dramatically increases its copy number. A particular method for this approach is based on the gTOW technique [18]. The genome-wide gTOW analysis has

revealed over 80% of the yeast genome with more than 100 copies of an upper limit of gene copy number.

The impact of an increase in gene copy number on cell fitness differs between doubled number of genes in an extra chromosome and many copies of a single gene. Previous studies have demonstrated that aneuploidy-induced proteotoxic stress causes cell fragility leading to growth impairment [15,24,25]. Because aneuploid yeast strains are very sensitive to perturbations at the RNA and protein levels, aneuploidy-induced proteotoxicity affects a wide range of biological processes. On the other hand, overexpression of most individual genes does not inhibit growth of wild-type yeast strain [17,18]. Thus, the gTOW technique allows us to study mechanisms for buffering against genetic perturbations by focusing on individual target genes in normal physiological condition. I expected that exploring the effects of an increase in individual gene copy number identifies novel mechanisms for maintaining cellular homeostasis. Indeed, a very recent study has shown that the fragility of aneuploid cells is caused by many genes on single additional chromosomes but not by duplicated dosage-sensitive genes that were identified by the gTOW analysis [23]. This study identified Mtw1 and Rpp1 as the dosage-compensated proteins that are not compensated in aneuploid cells [19]. This difference may result from aneuploidy-specific physiological conditions associated with proteotoxicity.

5.3 Quality control mechanisms for the assembly of multi-protein complexes

Recent studies investigating the robust formation of protein complexes have elucidated the location where subunits are translated [75,76], the timing when subunits are assembled into complexes [77], and the mechanisms by which subunit stoichiometry is maintained [30,70]. In agreement with previous studies [15,53,67,70,78,79], this study suggests the biological role of dosage compensation as robust formation of protein com-

plexes. Furthermore, this study identifies proteasomal degradation as a mechanism of the compensation and provides direct evidence for the ubiquitination of the individual dosage-compensated proteins (Figure 3.2C). Thus, these findings enhance our understanding of dosage compensation as a mechanism for the fine-tuning of subunit levels.

Protein-level dosage compensation seems to occur cotranslationally for the following reasons: (i) subunits are assembled into complexes cotranslationally [77], (ii) a large proportion of the proteome is cotranslationally ubiquitinated [80,81], and (iii) the degradation of subunits via an N-terminal acetylation at the nascent chain level has been supported by experimental evidence [70]. Because N-terminal acetylation is proposed to function as a degradation signal, a global analysis of N-terminal acetylation of proteins under genetic perturbations might provide insight into the sensing mechanism of the imbalance in subunit stoichiometries in complexes. Proteins containing N-terminal acetylation are targeted by the N-end rule pathway and subsequently polyubiquitinated and degraded through the ubiquitin–proteasome system [70,82]. Since polyubiquitination and proteasomal degradation of the dosage-compensated proteins are shown in this study, the analysis of N-terminal acetylation of these proteins may be helpful to investigate the contribution of the N-acetyltransferase to dosage compensation.

5.4 Concluding remark

Previous study has demonstrated that protein synthesis rate has correlation with stoichiometry of subunits in multi-protein complexes [30]. However, this study has also shown that some subunits are synthesized in excess, which indicates that translational control is not enough to guarantee subunit stoichiometry. Because some studies suggest that an imbalance in subunit stoichiometry relates with a decrease in cellular fitness [13,18,19,26], the cell should remove excess subunits in order to maintain cell growth.

As shown in this study, protein-level dosage compensation predominantly targets and degrades excess subunits through the ubiquitin–proteasome system. Therefore, dosage compensation may provide a reasonable explanation for maintenance of subunit stoichiometry. Here, I propose the two-layer mechanism for maintaining the correct stoichiometry of complex subunits (Figure 5.1). This two-layer mechanism seems to function as the fail-safe mechanism conferring robustness to cell systems. For validation of this model, it is critical to examine whether Srp54 and Sec65, subunits of signal recognition particle synthesized in excess [30], are subjected to dosage compensation.

This study has focused on the effects of gene copy number alterations on cellular robustness, and I applied the gTOW technique in order to manipulate and perturb gene expression. With this approach, I aimed to understand the mechanism for buffering against genetic perturbations and the quantitative aspects of the central dogma of molecular biology in the context of robustness. Although gene copy number was artificially increased in this study, changes in gene copy number are a common feature not only in disease conditions but also in physiological ones. Therefore, the implications of dosage compensation should be regarded as the potential contribution to cell robustness. Indeed, a very recent study has suggested that dosage compensation buffers the effect of transient changes in gene dosage during DNA replication on the resulting expression levels [83]. This study has shown that mRNA levels of early-replicating genes are down-regulated by acetylation of histone H3 K56 by Rtt109 and Asf1 and that the reduced mRNA levels are similar to those of late-replicating genes in *S. cerevisiae*. This observation suggests that dosage compensation has the broad impact on gene expression levels and implies that cells have to cope with gene-dosage imbalance, which is reviewed in [84].

A previous study has shown the possibility of manipulating dosage compensation in a chromosome-wide manner [85]. This study used induced pluripotent stem

cells derived from a Down's syndrome patient and introduced *XIST* gene, which is responsible for X-chromosome inactivation in mammalian cells, into one of the three chromosome 21 in the cells. Surprisingly, this resulted in widespread silencing of chromosome 21 at the mRNA level, indicating that this experiment has demonstrated translating dosage compensation to trisomy 21. One possible way to validate the controllability of the chromosome-wide dosage compensation is to examine the effects of the introduction of *XIST* gene to an aneuploid chromosome in cancer cells on gene expression levels from the target chromosome carrying *XIST* gene. If the gene expression levels are down-regulated, it may be strong evidence for *XIST* gene-dependent dosage compensation.

I conclude by noting that subunit stoichiometry potentially has a broad impact on robustness in cellular systems because of the fact that numerous biological processes are dependent on protein complexes. Furthermore, studies of mechanisms behind stoichiometry maintenance might be important for understanding diseases related to gene copy number alterations. For example, a recent study suggests that a set of specific genes on trisomic chromosome 21 have a causal effect on Down's syndrome [86]. Again, the approach based on the gTOW technique for measuring robustness in cellular systems provides a fundamental framework for the quantitative assessment of cell robustness.

5.5 Figure

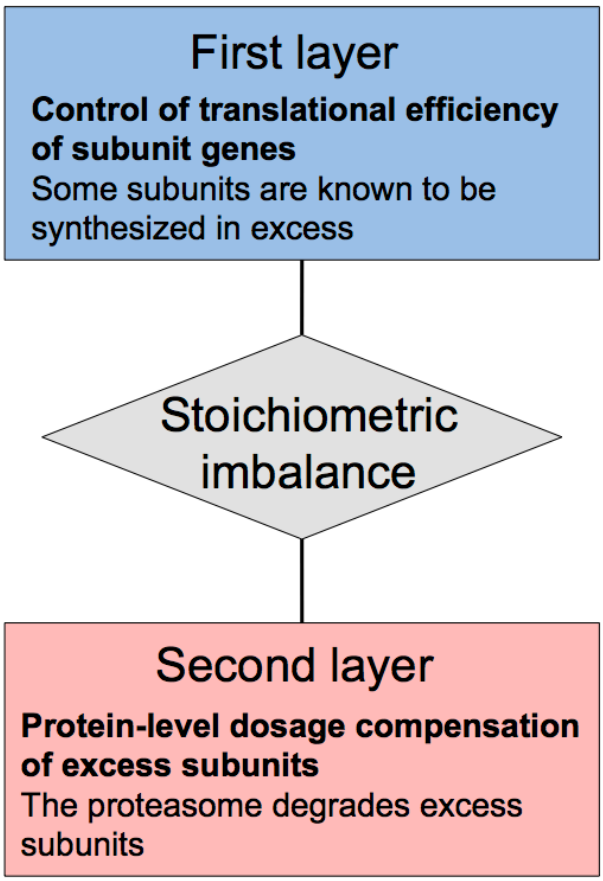

Figure 5.1. Model for the fail-safe mechanism contributing to cellular robustness. Translational control may be the predominant contribution to a balanced stoichiometry of complex subunits. As some studies have pointed out, stoichiometric imbalance may cause impaired cell growth, so that when subunits are translated in excess, cells may have to cope with the imbalanced stoichiometry. In this situation, protein-level dosage compensation may be responsible for regulating subunit stoichiometry in order to circumvent the growth defect. As this study has shown, the ubiquitin–proteasome system contributes to dosage compensation. Therefore, I believe that this two-layer mechanism, translational control and the ubiquitin–proteasome system, may function as the fail-safe mechanism.

Acknowledgments

First, I am deeply grateful to my mentor, Prof. Hisao Moriya. It was inspiring to discuss data and ideas with him. I am fortunate that he did not patronize me and frankly enjoyed my journey. He provided me many opportunities that encouraged my growth and helped to develop my professional career. The 7th ICYSB, a summer course in Sweden in 2015, was one of the opportunities, which led me to learn more about the Systems Biology and a global communication and meet wonderful friends.

I would like to appreciate to my adviser Prof. Kazuhiro Kutsukake for his support for this study and also for my student life. It enabled me to learn and study in an amazing environment.

I would also like to appreciate to my thesis advisors Prof. Sakae Takeuchi and Prof. Tatsuhiko Abo for their critical comments and questions on my study.

I would like to express my gratitude to Prof. Nick Ingolia and Dr. Shintaro Iwasaki for collaborating with Moriya laboratory and welcoming me when I visited Nick Ingolia laboratory at the UC Berkeley. I am sure that I will remember this experience repeatedly and encourage myself.

I would like to thank the Vincent J. Coates Genomics Sequencing Laboratory at the UC Berkeley for help with deep sequencing. I would also like to thank the National Bio-Resource Project in Japan for providing CMY765 strain (NBRP ID: BY22813). I thank Dr. Yuki Shimizu-Yoshida for providing strains. I would also like to thank to JSPS for a Grant-in-Aid for Research Fellow (16J00852).

I also thank members of the Moriya and Ingolia laboratories for advice and helpful discussions.

Finally, this thesis is dedicated to my family. They always encouraged and believed in me, even when I was in difficult situations.

Data Availability Statement

Ribosome profiling and RNA-seq data are available from the Gene Expression Omnibus under accession number GSE85036.

References

1. Kitano H, Oda K, Kimura T, Matsuoka Y, Csete M, Doyle J, et al. Metabolic syndrome and robustness tradeoffs. Diabetes. 2004;53(S3): S6-15. doi: 10.2337/diabetes.53.suppl_3.s6 pmid: 15561923
2. Stelling J, Sauer U, Szallasi Z, Doyle FJ, Doyle J. Robustness of cellular functions. Cell. 2004;118: 675–685. doi: 10.1016/j.cell.2004.09.008 pmid: 15369668
3. Kitano H. Towards a theory of biological robustness. Mol Syst Biol. 2007;3: 137. doi: 10.1038/msb4100179 pmid: 17882156
4. Masel J, Siegal ML. Robustness: mechanisms and consequences. Trends Genet. 2009;25: 395–403. doi: 10.1016/j.tig.2009.07.005 pmid: 19717203
5. Raj A, van Oudenaarden A. Nature, Nurture, or Chance: Stochastic Gene Expression and Its Consequences. Cell. 2008;135: 216–226. doi: 10.1016/j.cell.2008.09.050 pmid: 18957198
6. Balázsi G, van Oudenaarden A, Collins JJ. Cellular decision making and biological noise: From microbes to mammals. Cell. 2011;144: 910–925. doi: 10.1016/j.cell.2011.01.030 pmid: 21414483
7. Raser JM, O'Shea EK. Noise in gene expression: origins, consequences, and control. Science. 2005;309: 2010–3. doi: 10.1126/science.1105891 pmid: 16179466
8. Raj A, Rifkin SA, Andersen E, van Oudenaarden A. Variability in gene expression underlies incomplete penetrance. Nature. 2010;463: 913–8. doi: 10.1038/nature08781 pmid: 20164922
9. Gordon DJ, Resio B, Pellman D. Causes and consequences of aneuploidy in cancer. Nat Rev Genet. 2012;13: 189–203. doi: 10.1038/nrg3123 pmid: 22269907
10. Harper JW, Bennett EJ. Proteome complexity and the forces that drive proteome imbalance. Nature. 2016;537: 328–38. doi: 10.1038/nature19947 pmid: 27629639
11. Prelich G. Gene Overexpression: Uses, Mechanisms, and Interpretation. Genetics. 2012;190: 841–854. doi: 10.1534/genetics.111.136911 pmid: 22419077

12. Moriya H. Quantitative nature of overexpression experiments. Mol Biol Cell. 2015;26: 3932–3939. doi: 10.1091/mbc.E15-07-0512 pmid: 26543202
13. Oromendia AB, Amon A. Aneuploidy: implications for protein homeostasis and disease. Dis Model Mech. 2014;7: 15–20. doi: 10.1242/dmm.013391 pmid: 24396150
14. Deshaies RJ. Proteotoxic crisis, the ubiquitin-proteasome system, and cancer therapy. BMC Biol. 2014;12: 94. doi: 10.1186/s12915-014-0094-0 pmid: 25385277
15. Torres EM, Dephoure N, Panneerselvam A, Tucker CM, Whittaker CA, Gygi SP, et al. Identification of aneuploidy-tolerating mutations. Cell. 2010;143: 71–83. doi: 10.1016/j.cell.2010.08.038 pmid: 20850176
16. Oromendia AB, Dodgson SE, Amon A. Aneuploidy causes proteotoxic stress in yeast. Genes Dev. 2012;26: 2696–2708. doi: 10.1101/gad.207407.112 pmid: 23222101
17. Sopko R, Huang D, Preston N, Chua G, Papp B, Kafadar K, et al. Mapping pathways and phenotypes by systematic gene overexpression. Mol Cell. 2006;21: 319–330. doi: 10.1016/j.molcel.2005.12.011 pmid: 16455487
18. Makanae K, Kintaka R, Makino T, Kitano H, Moriya H. Identification of dosage-sensitive genes in Saccharomyces cerevisiae using the genetic tug-of-war method. Genome Res. 2013;23: 300–311. doi: 10.1101/gr.146662.112 pmid: 23275495
19. Dephoure N, Hwang S, O'Sullivan C, Dodgson SE, Gygi SP, Amon A, et al. Quantitative proteomic analysis reveals posttranslational responses to aneuploidy in yeast. Elife. 2014;3: e03023. doi: 10.7554/eLife.03023 pmid: 25073701
20. Keren L, Hausser J, Lotan-Pompan M, Vainberg Slutskin I, Alisar H, Kaminski S, et al. Massively Parallel Interrogation of the Effects of Gene Expression Levels on Fitness. Cell. 2016;166: 1282–1294.e18. doi: 10.1016/j.cell.2016.07.024 pmid: 27545349
21. Moriya H, Shimizu-Yoshida Y, Kitano H. In vivo robustness analysis of cell division cycle genes in Saccharomyces cerevisiae. PLoS Genet. 2006;2(7): e111. doi: 10.1371/journal.pgen.0020111 pmid: 16839182
22. Kaizu K, Moriya H, Kitano H. Fragilities caused by dosage imbalance in regulation of the budding yeast cell cycle. PLoS Genet. 2010;6(4): e1000919.

doi: 10.1371/journal.pgen.1000919 pmid: 20421994

23. Bonney ME, Moriya H, Amon A. Aneuploid proliferation defects in yeast are not driven by copy number changes of a few dosage-sensitive genes. Genes Dev. 2015;29: 898–903. doi: 10.1101/gad.261743.115 pmid: 25934502
24. Torres EM, Williams BR, Amon A. Aneuploidy: Cells losing their balance. Genetics. 2008;179: 737–746. doi: 10.1534/genetics.108.090878 pmid: 18558649
25. Torres EM, Sokolsky T, Tucker CM, Chan LY, Boselli M, Dunham MJ, et al. Effects of aneuploidy on cellular physiology and cell division in haploid yeast. Science. 2007;317: 916–24. doi: 10.1126/science.1142210 pmid: 17702937
26. Papp B, Pál C, Hurst LD. Dosage sensitivity and the evolution of gene families in yeast. Nature. 2003;424: 194–197. doi: 10.1038/nature01771 pmid: 12853957
27. Donnelly N, Storchová Z. Dynamic karyotype, dynamic proteome: Buffering the effects of aneuploidy. Biochim Biophys Acta - Mol Cell Res. 2014;1843: 473–481. doi: 10.1016/j.bbamcr.2013.11.017 pmid: 24295790
28. Katz W, Weinstein B, Solomon F. Regulation of tubulin levels and microtubule assembly in Saccharomyces cerevisiae: consequences of altered tubulin gene copy number. Mol Cell Biol. 1990;10: 5286–5294. doi: 10.1128/MCB.10.10.5286.Updated pmid: 2204811
29. Ingolia NT, Ghaemmaghami S, Newman JRS, Weissman JS. Genome-wide analysis in vivo of translation with nucleotide resolution using ribosome profiling. Science. 2009;324: 218–23. doi: 10.1126/science.1168978 pmid: 19213877
30. Li GW, Burkhardt D, Gross C, Weissman JS. Quantifying absolute protein synthesis rates reveals principles underlying allocation of cellular resources. Cell. 2014;157: 624–635. doi: 10.1016/j.cell.2014.02.033 pmid: 24766808
31. Crick F. Central Dogma of Molecular Biology. Nature. 1970;227: 561–563. doi: 10.1038/227561a0 pmid: 4913914
32. Brachmann CB, Davies A, Cost GJ, Caputo E, Li J, Hieter P, et al. Designer deletion strains derived from Saccharomyces cerevisiae S288C: A useful set of strains and plasmids for PCR-mediated gene disruption and other applications. Yeast. 1998;14: 115–132. doi: 10.1002/(SICI)1097-0061(19980130)14:2<115::AID-YEA204>3.0.CO;2-2 pmid: 9483801

33. Ghaemmaghami S, Huh WK, Bower K, Howson RW, Belle A, Dephoure N, et al. Global analysis of protein expression in yeast. Nature. 2003;425: 737–41. doi: 10.1038/nature02046 pmid: 14562106
34. Amberg DC, Burke D, Strathern JN. Methods in Yeast Genetics: A Cold Spring Harbor Laboratory Course Manual. Cold Spring Harbor Laboratory Press; 2005.
35. Chino A, Makanae K, Moriya H. Relationships between Cell Cycle Regulator Gene Copy Numbers and Protein Expression Levels in Schizosaccharomyces pombe. PLoS One. 2013;8(9): e73319. doi: 10.1371/journal.pone.0073319 pmid: 24019917
36. Köhrer K, Domdey H. Preparation of high molecular weight RNA. Methods Enzymol. 1991;194: 398–405. pmid: 1706459
37. Huh W-K, Falvo JV., Gerke LC, Carroll AS, Howson RW, Weissman JS, et al. Global analysis of protein localization in budding yeast. Nature. 2003;425: 686–691. doi: 10.1038/nature02026 pmid: 14562095
38. Carpenter AE, Jones TR, Lamprecht MR, Clarke C, Kang IH, Friman O, et al. CellProfiler: image analysis software for identifying and quantifying cell phenotypes. Genome Biol. 2006;7: R100. doi: 10.1186/gb-2006-7-10-r100 pmid: 17076895
39. Chong YT, Koh JLY, Friesen H, Duffy K, Cox MJ, Moses A, et al. Yeast proteome dynamics from single cell imaging and automated analysis. Cell. 2015;161: 1413–1424. doi: 10.1016/j.cell.2015.04.051 pmid: 26046442
40. Cherry JM, Ball C, Weng S, Juvik G, Schmidt R, Adler C, et al. Genetic and physical maps of Saccharomyces cerevisiae. Nature. 1997;387: 67–73. pmid: 9169866
41. Okamoto K. Organellophagy: Eliminating cellular building blocks via selective autophagy. J Cell Biol. 2014;205: .
42. Lu K, Psakhye I, Jentsch S. Autophagic clearance of PolyQ proteins mediated by ubiquitin-Atg8 adaptors of the conserved CUET protein family. Cell. 2014;158: 549–563. doi: 10.1016/j.cell.2014.05.048 pmid: 25042851
43. Kraft C, Deplazes A, Sohrmann M, Peter M. Mature ribosomes are selectively degraded upon starvation by an autophagy pathway requiring the Ubp3p/Bre5p ubiquitin protease. Nat Cell Biol. 2008;10: 602–610. doi: 10.1038/ncb1723
44. Stingele S, Stoehr G, Peplowska K, Cox J, Mann M, Storchova Z. Global

analysis of genome, transcriptome and proteome reveals the response to aneuploidy in human cells. Mol Syst Biol. 2012;8: 608. doi: 10.1038/msb.2012.40 pmid: 22968442

45. Santaguida S, Vasile E, White E, Amon A. Aneuploidy-induced cellular stresses limit autophagic degradation. Genes Dev. 2015;29: 2010–2021. doi: 10.1101/gad.269118.115 pmid: 26404941

46. Thorburn RR, Gonzalez C, Brar GA, Christen S, Carlile TM, Ingolia NT, et al. Aneuploid yeast strains exhibit defects in cell growth and passage through START. Mol Biol Cell. 2013;24: 1274–89. doi: 10.1091/mbc.E12-07-0520 pmid: 23468524

47. Remacha M, Jimenez-Diaz A, Bermejo B, Rodriguez-Gabriel MA, Guarinos E, Ballesta JPG. Ribosomal acidic phosphoproteins P1 and P2 are not required for cell viability but regulate the pattern of protein expression in Saccharomyces cerevisiae. Mol Cell Biol. 1995;15: 4754–4762. doi: 10.1128/MCB.15.9.4754 pmid: 7651393

48. Ghislain M, Udvardy A, Mann C. S. cerevisiae 26S protease mutants arrest cell division in G2/metaphase. Nature. 1993;366: 358–362. doi: 10.1038/366358a0 pmid: 8247132

49. Leporé N, Lafontaine DLJ. A functional interface at the rDNA connects rRNA synthesis, pre-rRNA processing and nucleolar surveillance in budding yeast. PLoS One. 2011;6(9): e24962. doi: 10.1371/journal.pone.0024962 pmid: 21949810

50. Ingolia NT, Brar GA, Rouskin S, McGeachy AM, Weissman JS. The ribosome profiling strategy for monitoring translation in vivo by deep sequencing of ribosome-protected mRNA fragments. Nat Protoc. 2012;7: 1534–1550. doi: 10.1038/nprot.2012.086 pmid: 22836135

51. Iwasaki S, Floor SN, Ingolia NT. Rocaglates convert DEAD-box protein eIF4A into a sequence-selective translational repressor. Nature. 2016;1–17. doi: 10.1038/nature17978 pmid: 27309803

52. Anders S, Huber W. Differential expression analysis for sequence count data. Genome Biol. 2010;11: R106. doi: 10.1186/gb-2010-11-10-r106 pmid: 20979621

53. Singh RK, Kabbaj MHM, Paik J, Gunjan A. Histone levels are regulated by phosphorylation and ubiquitylation-dependent proteolysis. Nat Cell Biol.

2009;11: 925–33. doi: 10.1038/ncb1903 pmid: 19578373

54. Korolchuk VI, Menzies FM, Rubinsztein DC. A novel link between autophagy and the ubiquitin-proteasome system. Autophagy. 2009;5: 862–863. doi: 10.4161/auto.8840

55. Korolchuk VI, Menzies FM, Rubinsztein DC. Mechanisms of cross-talk between the ubiquitin-proteasome and autophagy-lysosome systems. FEBS Lett. 2010;584: 1393–1398. doi: 10.1016/j.febslet.2009.12.047

56. Zhang T, Shen S, Qu J, Ghaemmaghami S. Global Analysis of Cellular Protein Flux Quantifies the Selectivity of Basal Autophagy. Cell Rep. 2016;14: 2426–2439. doi: 10.1016/j.celrep.2016.02.040 pmid: 26947064

57. Gorenstein C, Warner JR. Synthesis and Turnover of Ribosomal Proteins in the Absence of 60S Subunit Assembly in Saccharomyces cerevisiae. Molec gen Genet. 1977;157: 327–332.

58. Sung M-K, Reitsma JM, Sweredoski MJ, Hess S, Deshaies RJ. Ribosomal proteins produced in excess are degraded by the ubiquitin-proteasome system. Mol Biol Cell. 2016;mbcE16-05-0290. doi: 10.1091/mbc.E16-05-0290 pmid: 27385339

59. Springer M, Weissman JS, Kirschner MW. A general lack of compensation for gene dosage in yeast. Mol Syst Biol. 2010;6: 368. doi: 10.1038/msb.2010.19 pmid: 20461075

60. Houser-Scott F, Xiao S, Millikin CE, Zengel JM, Lindahl L, Engelke DR. Interactions among the protein and RNA subunits of Saccharomyces cerevisiae nuclear RNase P. Proc Natl Acad Sci U S A. 2002;99: 2684–9. doi: 10.1073/pnas.052586299 pmid: 11880623

61. Aspinall TV, Gordon JMB, Bennett HJ, Karahalios P, Bukowski JP, Walker SC, et al. Interactions between subunits of Saccharomyces cerevisiae RNase MRP support a conserved eukaryotic RNase P/MRP architecture. Nucleic Acids Res. 2007;35: 6439–6450. doi: 10.1093/nar/gkm553 pmid: 17881380

62. Lygerou Z, Mitchell P, Petfalski E, Séraphin B, Tollervey D. The POP1 gene encodes a protein component common to the RNase MRP and RNase P ribonucleoproteins. Genes Dev. 1994;8: 1423–1433. doi: 10.1101/gad.8.12.1423 pmid: 7926742

63. Dichtl B, Tollervey D. Pop3p is essential for the activity of the RNase MRP and

RNase P ribonucleoproteins in vivo. EMBO J. 1997;16: 417–429. doi: 10.1093/emboj/16.2.417 pmid: 9029160

64. Chu S, Zengel JM, Lindahl L. A novel protein shared by RNase MRP and RNase P. RNA. 1997;3: 382–91. pmid: 9085845

65. Stolc V, Altman S. Rpp1, an essential protein subunit of nuclear RNase P required for processing of precursor tRNA and 35S precursor rRNA in Saccharomyces cerevisiae. Genes Dev. 1997;11: 2414–25. doi: 10.1101/gad.11.18.2414 pmid: 9308968

66. Chamberlain JR, Lee Y, Lane WS, Engelke DR. Purification and characterization of the nuclear RNase P holoenzyme complex reveals extensive subunit overlap with RNase MRP. Genes Dev. 1998;12: 1678–1690. doi: 10.1101/gad.12.11.1678 pmid: 9620854

67. Mueller S, Wahlander A, Selevsek N, Otto C, Ngwa EM, Poljak K, et al. Protein degradation corrects for imbalanced subunit stoichiometry in OST complex assembly. Mol Biol Cell. 2015;26: 2596–2608. doi: 10.1091/mbc.E15-03-0168 pmid: 25995378

68. Schwarz M, Knauer R, Lehle L. Yeast oligosaccharyltransferase consists of two functionally distinct sub-complexes, specified by either the Ost3p or Ost6p subunit. FEBS Lett. 2005;579: 6564–6568. doi: 10.1016/j.febslet.2005.10.063 pmid: 16297388

69. Knauer R, Lehle L. The oligosaccharyltransferase complex from Saccharomyces cerevisiae. Isolation of the OST6 gene, its synthetic interaction with OST3, and analysis of the native complex. J Biol Chem. 1999;274: 17249–56. doi: 10.1074/JBC.274.24.17249 pmid: 10358084

70. Shemorry A, Hwang CS, Varshavsky A. Control of Protein Quality and Stoichiometries by N-Terminal Acetylation and the N-End Rule Pathway. Mol Cell. 2013;50: 540–551. doi: 10.1016/j.molcel.2013.03.018 pmid: 23603116

71. Francis SM, Gas ME, Daugeron MC, Bravo J, Séraphin B. Rbg1-Tma46 dimer structure reveals new functional domains and their role in polysome recruitment. Nucleic Acids Res. 2012;40: 11110–11114. doi: 10.1093/nar/gks867 pmid: 23002146

72. De Wulf P, McAinsh AD, Sorger PK. Hierarchical assembly of the budding yeast kinetochore from multiple subcomplexes. Genes Dev. 2003;17: 2902–2921. doi:

10.1101/gad.1144403 pmid: 14633972

73. Li F, Dong J, Eichmiller R, Holland C, Minca E, Prakash R, et al. Role of Saw1 in Rad1/Rad10 complex assembly at recombination intermediates in budding yeast. EMBO J. 2013;32: 461–72. doi: 10.1038/emboj.2012.345 pmid: 23299942
74. Marzioch M, Henthorn DC, Herrmann JM, Wilson R, Thomas DY, Bergeron JJM, et al. Erp1p and Erp2p, partners for Emp24p and Erv25p in a yeast p24 complex. Mol Biol Cell. 1999;10: 1923–1938. doi: 10.1091/mbc.10.6.1923 pmid: 10359606
75. Williams CC, Jan CH, Weissman JS. Targeting and plasticity of mitochondrial proteins revealed by proximity-specific ribosome profiling. Science. 2014;346: 748–51. doi: 10.1126/science.1257522 pmid: 25378625
76. Jan CH, Williams CC, Weissman JS. Principles of ER cotranslational translocation revealed by proximity-specific ribosome profiling. Science. 2014;346: 1257521–1257521. doi: 10.1126/science.1257521 pmid: 25378630
77. Shieh YW, Minguez P, Bork P, Auburger JJ, Guilbride DL, Kramer G, et al. Operon structure and cotranslational subunit association direct protein assembly in bacteria. Science. 2015;350: 678–680. doi: 10.1126/science.aac8171 pmid: 26405228
78. Chen J, Archer TK. Regulating SWI / SNF Subunit Levels via Protein-Protein Interactions and Proteasomal Degradation: BAF155 and BAF170 Limit Expression of BAF57. Gene Expr. 2005;25: 9016–9027. doi: 10.1128/MCB.25.20.9016-9027.2005 pmid: 16199878
79. Sung MK, Reitsma JM, Sweredoski MJ, Hess S, Deshaies RJ. Ribosomal proteins produced in excess are degraded by the ubiquitin-proteasome system. Mol Biol Cell. 2016;mbcE16-05-0290. doi: 10.1091/mbc.E16-05-0290 pmid: 27385339
80. Duttler S, Pechmann S, Frydman J. Principles of cotranslational ubiquitination and quality control at the ribosome. Mol Cell. 2013;50: 379–393. doi: 10.1016/j.molcel.2013.03.010 pmid: 23583075
81. Wang F, Durfee LA, Huibregtse JM. A cotranslational ubiquitination pathway for quality control of misfolded proteins. Mol Cell. 2013;50: 368–378. doi: 10.1016/j.molcel.2013.03.009 pmid: 23583076
82. Hwang C-S, Shemorry A, Varshavsky A. N-Terminal Acetylation of Cellular

Proteins Creates Specific Degradation Signals. Science (80-). 2010;327: 973–977. doi: 10.1126/science.1183147 pmid: 20110468

83. Voichek Y, Bar-Ziv R, Barkai N. Expression homeostasis during DNA replication. Science (80-). 2016;351: 1087–1090. doi: 10.1126/science.aad1162 pmid: 26941319

84. Bar-Ziv R, Voichek Y, Barkai N. Dealing with Gene-Dosage Imbalance during S Phase. Trends Genet. 2016;32: 717–723. doi: 10.1016/j.tig.2016.08.006 pmid: 27575299

85. Jiang J, Jing Y, Cost GJ, Chiang J-C, Kolpa HJ, Cotton AM, et al. Translating dosage compensation to trisomy 21. Nature. 2013;500: 296–300. doi: 10.1038/nature12394 pmid: 23863942

86. Makino T, McLysaght A. Ohnologs in the human genome are dosage balanced and frequently associated with disease. Proc Natl Acad Sci U S A. 2010;107: 9270–4. doi: 10.1073/pnas.0914697107 pmid: 20439718

List of Publications

1. Koji Makanae, Reiko Kintaka, Koji Ishikawa, Hisao Moriya. (2015) Small Toxic Protein Encoded on Chromosome VII of *Saccharomyces cerevisiae*. *PLoS One*, 10(3): e0120678.
2. Koji Ishikawa, Koji Makanae, Shintaro Iwasaki, Nicholas T. Ingolia, Hisao Moriya. (2017) Post-Translational Dosage Compensation Buffers Genetic Perturbations to Stoichiometry of Protein Complexes. *PLoS Genetics*, 13(1): e1006554.
3. Koji Ishikawa, Yuichi Eguchi, Hisao Moriya. (2017) Measuring Intracellular Parameters. *Experimental Medicine*, Vol.35 No.5.